Alkali Metal Cation−π Interactions Observed by Using a Lariat Ether Model System

Eric S. Meadows,[†] Stephen L. De Wall,[†] Leonard J. Barbour,[‡] and George W. Gokel*,[†]

Contribution from the Bioorganic Chemistry Program and Department of Molecular Biology & Pharmacology, Washington University School of Medicine, 660 South Euclid Avenue, Campus Box 8103, St. Louis, Missouri 63110, and Department of Chemistry, University of Missouri, 601 South College Avenue, Columbia, Missouri 65211

Received August 16, 2000

Abstract: The Na^+ or K^+ cation−π interaction has been experimentally probed by using synthetic receptors that comprise diaza-18-crown-6 lariat ethers having ethylene sidearms attached to aromatic π-donors. The side chains are 2-(3-indolyl)ethyl (**7**), 2-(3-(1-methyl)indolyl)ethyl (**8**), 2-(3-(5-methoxy)indolyl)ethyl (**9**), 2-(4-hydroxyphenyl)ethyl (**10**), 2-phenylethyl (**11**), 2-pentafluorophenylethyl (**12**), and 2-(1-naphthyl)ethyl (**13**). Solid-state structures are reported for six examples of alkali metal complexes in which the cation is π-coordinated by phenyl, phenol, or indole. Indole-containing crown, **7**, adopts a similar conformation when bound by NaI, KI, KSCN, or KPF_6. In each case, the macroring and both arenes coordinate the cation; the counteranion is excluded from the solvation sphere. NMR measurements in acetone-d_6 solution confirm the observed solid-state conformations of unbound **7** and **7**·NaI. In **7**·Na^+ and **7**·K^+, the pyrrolo, rather than benzo, subunit of indole is the π-donor for the alkali metal cation. Cation−π complexes were also observed for **10**·KI and **11**·KI. In these cases, the orientation of the cation on the aromatic ring is in accord with the binding site predicted by computational studies. In contrast to the phenyl case (**11**) the pentafluorophenyl group of **12** failed to coordinate K^+. Solid-state structures are also reported for **7**·$NaPF_6$, **10**·NaI, **11**·NaI, **13**·KI, **13**·KPF_6, and **9**·NaI, in which cation−π complexation is not observed. Steric and electrostatic considerations in the π-complexation of alkali metal cations by these lariat ethers are thought to account for the observed complexation behavior or lack thereof.

Introduction

Prior to the late 1960's, the experimental study of alkali metal cation chemistry was difficult at best. The advent of crown ethers[1] and cryptands[2] provided a vehicle for such studies and the field has since burgeoned. Numerous studies have defined the π-donor abilities of a variety of elements such as O, N, and S toward alkali metal cations. Assessing the ability of π-donors to interact with alkali metals has proved elusive. The importance of alkali metal cation−π interactions is potentially great, especially in biological systems where nearly 10% of amino acid side chains are terminated by the aromatic residues benzene (in phenylalanine, Phe, F), phenol (in tyrosine, Tyr, Y), and indole (in tryptophan, Trp, W).

Experimental evidence for cation−π interactions dates from the pioneering work of Kebarle and co-workers,[3] who showed that the coordination of K^+ by a molecule of benzene or of water in the gas phase was approximately isoenergetic. More recent work from the laboratories of Castleman[4] and Lisy[5] has confirmed these findings and extended them to Na^+. Hoffmann and Weiss had, even earlier, reported a solid-state structure of $KBPh_4$ in which K^+ was cradled between two benzene rings.[6] Atwood and co-workers reported a structure in which an apical interaction between a molecule of benzene and a crown-complexed K^+ cation appeared to stabilize the latter.[7] Our own efforts to develop lariat ether receptors that could be used to assess π-interactions between alkali metal cations and double or triple bonds appeared encouraging at first but thermodynamic and solid-state analyses ultimately failed to confirm them.[8] Novel solid-state studies in the cation−π complexation arena continue to emerge.[9]

Interest in cation−π interactions was stimulated in the 1990's by a postulate that the aromatic side chains of amino acids might determine K^+ transport selectivity in transmembrane protein channels.[10] Site-directed mutagenesis studies by Heginbotham and MacKinnon permitted a test of this postulate by removal of the hydroxyl group from a critical tyrosine residue. The phenol (Tyr) to phenyl (Phe, i.e. Y → F) mutation removed the hydroxyl group but left the arene in tact. Cation transport selectivity was altered in the mutant even though the arene was

[†] Washington University School of Medicine.
[‡] University of Missouri.

(1) Pedersen, C. J. *J. Am. Chem. Soc.* **1967**, *89*, 2495, 7017.
(2) (a) Dietrich, B.; Lehn, J. M.; Sauvage, J. P. *Tetrahedron Lett.* **1969**, 2885. (b) Lehn, J. M.; Sauvage, J. P. *J. Chem. Soc., Chem. Commun.* **1971**, 440.
(3) Sunner, J.; Nishizawa, K.; Kebarle, P. *J. Phys. Chem.* **1981**, *85*, 1814−1820.
(4) Guo, B. C.; Purnell, J. W.; Castleman, A. W., Jr. *Chem. Phys. Lett.* **1990**, *168*, 155−160.
(5) (a) Cabarcos, O. M.; Weinheimer, C. J.; Lisy, J. M. *J. Chem. Phys.* **1998**, *108*, 5151−5154. (b) Cabarcos, O. M.; Weinheimer, C. J.; Lisy, J. M. *J. Chem. Phys.* **1999**, *110*, 8429−8435.
(6) Hoffmann, K.; Weiss, E. *J. Organomet. Chem.* **1974**, *67*, 221−8.
(7) (a) Atwood, J. L.; Crissinger, K. D.; Rogers, R. D. *J. Organomet. Chem.* **1978**, *155*, 1−14. (b) Hrncir, D. C.; Rogers, R. D.; Atwood, J. L. *J. Am. Chem. Soc.* **1981**, *103*, 4277−8. (c) Atwood, J. L. *J. Inclusion Phenom.* **1985**, *3*, 13−20.
(8) Arnold, K. A.; Viscariello, A. M.; Kim, M.-S.; Gandour, R. A.; Fronczek, F. R.; Gokel, G. W. *Tetrahedron Lett.* **1988**, 3025−3028.
(9) King, B. T.; Noll, B. C.; Michl, J. *Collect. Czech. Chem. Commun.* **1999**, *64*, 1001−1012.
(10) Kumpf, R. A.; Dougherty, D. A. *Science* **1993**, *261*, 1708−1710.

10.1021/ja003059e CCC: $20.00
Published on Web 03/08/2001

still present.[11] The recently reported solid-state structure of the KcsA K^+ channel of *Streptomyces lividans* shows that the tyrosine hydroxyl group rather than the arene plays a key structural role.[12]

The importance of cation−π interactions[13] looms large in biology. In the nonpolar interior of a protein, such interactions may be significant. The three amino acids phenylalanine, tyrosine, and tryptophan have abundances in all known proteins of 3.9%, 3.2%, and 1.3%, respectively. In any given protein, 8.4% of the amino acids may be involved in cation−π interactions. This means that a protein having 250 amino acids could theoretically have as many as 21 alkali metal−arene contacts in a single molecule. The potential importance of such interactions and the need to understand them at the molecular level is clear.

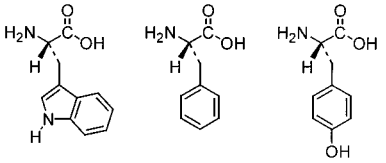

A

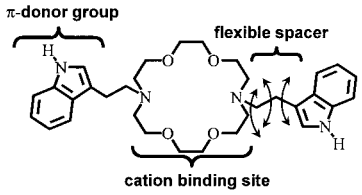

B

An important and related question is that of ammonium−π interactions, discussed in an early article by Kier and Aldrich.[14] They attempted to understand the effect of ammonium ion interactions on the binding of drugs to protein receptors and in model systems such as the methylamine·indole complex. In a second report,[15] influenced by earlier proposals by O'Brien,[16] they conducted calculations to assess the binding of small molecule models to acetylcholinesterase. The calculated binding energy was then used to compute a theoretical catalytic rate, which was compared to the experimentally determined value. By studying charged and hydrophobic substrates, they found that an anionic binding site could not account for the experimentally observed rates. Instead, the best agreement with experiment was obtained by using a model in which aromatic residues dominated the binding of the tertiary nitrogen of acetylcholine. The presence of the aromatic binding site was confirmed by the X-ray structure determination of the enzyme[17] and inhibitor−enzyme complexes.[18] The stabilization mechanism was thought to involve induced dipoles rather than cation−π interactions, but the relevance of this effort is obvious. A similar binding mechanism has been suggested for the nicotinic acetylcholine receptor, which is an ion channel.[19] In the work described below, we report experimental evidence that clearly confirms the cation−π interaction of benzene, indole, and phenol with K^+. Fewer data are available for the Na^+−arene interaction but this is demonstrated as well.

Results

Receptors Used in This Study. Compounds **2**−**13** are bibracchial (2-armed) lariat ethers.[20] All are diaza-18-crown-6 derivatives that have two identical sidearms. The crown ether system was chosen because it affords a well-characterized binding site for alkali metal cations such as Na^+ and K^+. The receptor sidearms were designed to be sufficiently flexible to turn either inward or outward depending on the system's demands. Compounds **3**−**6** have single carbon spacers connecting the macroring to an unsaturated residue. Receptors **2**−**6** were studied previously and found not to exhibit cation−π complexation as judged by solution thermodynamic and X-ray diffraction studies.[21] A subsequent study of molecular models suggested that a 2-carbon chain would provide optimal spacing for the formation of an intramolecular π-complex. Three receptors in particular, **7**, **10**, and **11**, were chosen because the pendant residues correspond to the side chains of the aromatic amino acids tryptophan (⇒ **7**), tyrosine (⇒ **10**), and phenylalanine (⇒ **11**).

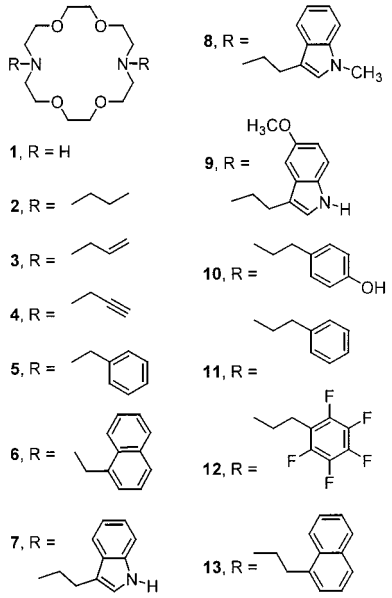

Choice of Crown Ether. A decision was made at an early stage to use a substituted diazacrown as the receptor's basic scaffold. Sidearms attached to nitrogen may complex from the same or opposite sides of the macroring due to nitrogen's ability to undergo rapid inversion. If the sidearms were attached at carbon, the receptor would exhibit "sidedness". There is also

(11) Heginbotham, L.; Lu, Z.; Abramson, T.; MacKinnon, R. *Biophys. J.* **1994**, *66*, 1061.
(12) Doyle, D. A.; Cabral, J. M.; Pfuetzner, R. A.; Kuo, A.; Gulbis, J. M.; Cohen, S. L.; Chait, B. T.; MacKinnon, R. *Science* **1998**, *280*, 69−77.
(13) Ma, J. C.; Dougherty, D. A. *Chem. Rev.* **1997**, *97*, 1303−1324.
(14) Kier, L. B.; Aldrich, H. S. *J. Theor. Biol.* **1974**, *46*, 529−41.
(15) Hoeltje, H. D.; Kier, L. B. *J. Pharm. Sci.* **1975**, *64*, 418−20.
(16) O'Brien, R. D. *Med. Chem. Ser. Monogr.* **1971**, *11*, 161−212.
(17) Sussman, J. L.; Harel, M.; Frolow, F.; Oefner, C.; Goldman, A.; Toker, L.; Silman, I. *Science* **1991**, *253*, 872−879.
(18) (a) Silman, I.; Harel, M.; Axelsen, P.; Raves, M.; Sussman, J. L. *Biochem. Soc. Trans.* **1994**, *22*, 745−9. (b) Eichler, J.; Anselmet, A.; Sussman, J. L.; Massoulie, J.; Silman, I. *Mol. Pharmacol.* **1994**, *45*, 335−40. (c) Harel, M.; Schalk, I.; Ehret-Sabatier, L.; Bouet, F.; Goeldner, M.; Hirth, C.; Axelsen, P. H.; Silman, I.; Sussman, J. L. *Proc. Natl. Acad. Sci. U.S.A.* **1993**, *90*, 9031−9035. (d) Ripoll, D. R.; Faerman, C. H.; Axelsen, P. H.; Silman, I.; Sussman, J. L. *Proc. Natl. Acad. Sci. U.S.A.* **1993**, *90*, 5128−32.
(19) Zhonge, W.; Gallivan, J. P.; Zhang, Y.; Li, L.; Lester, H. A.; Dougherty, D. A. *Proc. Natl. Acad. Sci. U.S.A.* **1998**, *95*, 12088−12093 and references therein.
(20) (a) Gokel, G. W. *Chem. Soc. Rev.* **1992**, *21*, 39−47. (b) Gokel, G. W.; Schall, O. F. Lariat Ethers. In *Comprehensive Supramolecular Chemistry*; Elsevier: Oxford, 1996; pp 97−152.
(21) Arnold, K. A.; Viscariello, A. M.; Kim, M.; Gandour, R. D.; Fronczek, F. R.; Gokel, G. W. *Tetrahedron Lett.* **1988**, 3025−3028.

an inherent economy in such structures since the nitrogen atom serves as both a pivot atom and a macroring donor group.

Either 15- or 18-membered diazacrowns[22] could have been the basic subunit for the receptor. The choice of the 18-membered ring system was made based on three issues. First, sidearms attached at the macroring nitrogens of diaza-18-crown-6 can interact in a symmetric fashion that is not possible for the 15-membered-ring compounds. Second, the presence of a sixth donor in the 18-membered ring generally enhances the cation-binding strength for alkali metal cations. This increase is generally an order of magnitude in anhydrous CH_3OH solution and more in less polar solvents. Third, many more crystal structures are known for 18-membered-ring complexes than for the 15-membered relatives. This may be due to the fact that synthetic access is better for the 18-membered-ring systems and more receptors are available. In our experience the 18-membered-ring complexes generally crystallize more readily than do the 15-membered-ring analogues. In any event, the existence of more 18-membered-ring examples makes for better comparisons.

Linker Length. Early studies,[8] in which we sought to identify interactions of alkali metal cations with double or triple bonds or benzene, used one-carbon spacers between the arene and macroring. Thus the sidearms attached to nitrogen in 4,13-diaza-18-crown-6 were allyl (**3**), propargyl (**4**), and benzyl (**5**), respectively. Solid-state structures of **3**−**6** complexing Na^+ or K^+ failed to show sidearm involvement. Successful alkali metal complexation was achieved when, for example, an oxygen donor was placed 2 carbons distant from the nitrogen. In the present studies 2-carbon, rather than 1-carbon, spacer units were favored.

The use of 3-carbon linker arms was considered but deferred until results were obtained for the 2-carbon spacer systems, **7**, **10**, and **11**. The 3-carbon linker would provide additional extension if required but could potentially suffer from unfavorable conformational (gauche) interactions in the linker chain. We felt it best to avoid unnecessary conformational variables at the early stage of the project.

Molecular models (CPK) were prepared of compounds **1**−**13**. For the present study, particular attention was paid to macrocycles in which the sidearms corresponded to aromatic amino acid side chains: 2-(3-indolyl)ethyl (**7**), 2-(4-hydroxyphenyl)-ethyl (**10**), and 2-phenylethyl (**11**). The design of the system required a cation (Na^+ or K^+) to be bound by the macroring. The sidearm needed to be long enough and sufficiently flexible to permit the arene to occupy the vacant apical coordination sites. We assumed that the coordination sphere would be a hexagonal bipyramid in which the crown ether affords the equatorial donors.

For compounds **7**, **10**, and **11**, this was the case. In the 2-(3-indolyl)ethyl (**7**) case, a further issue was considered. The ring-bound cation's apical position could be occupied by either the benzene or pyrrole centroid of indole. Theoretical calculations suggested that the most favorable electrostatic potential is found in the benzene, rather than the pyrrole ring; the former is predicted to be the preferred donor site. Molecular models suggested that a conformation in which the benzene rings could serve as apical donors on opposite sides of the macroring was readily accessible.

Sidearm Structural Features. Computational studies have shown that among the aromatic amino acids (His, Phe, Trp, Tyr), tryptophan (i.e. indole) has the greatest cation−π donicity.[23] Thus indole was used as the π-donor system in the first synthetic receptor prepared, **7**.[24] More recently, phenol and phenyl, the side chains of Tyr and Phe, have been incorporated into receptors (**10** and **11**, respectively).[25] Pentafluorophenyl derivative **12** was designed to maintain the aromaticity of **11** but to reverse the arene's electrostatic potential surface (see below), thereby reducing the sidearm's π-donicity. Compounds **8** (*N*-methylindolylethyl sidearms), **9** (5-methoxyindolylethyl sidearms), and **13** (1-naphthylethyl sidearms) were all designed to be analogues of **7**. *N*-Methyl- and 5-methoxyindole derivatives **8** and **9** are obvious derivatives of **7**. The 5-methoxyindole receptor, **9**, was designed to increase the cation−π donicity of indole. The *N*-Me indole receptor (**8**) was prepared to probe the effect of preventing the indole from participating in a hydrogen bond with an anion or solvent. In **13**, the pyrrolo ring of **7** is replaced by a second benzene ring. In a sense, **13** is an analogue of both **7** and **11**. The centroids of the two six-membered rings of naphthalene provide two equivalent π donor sites on each sidearm.

Scheme 1

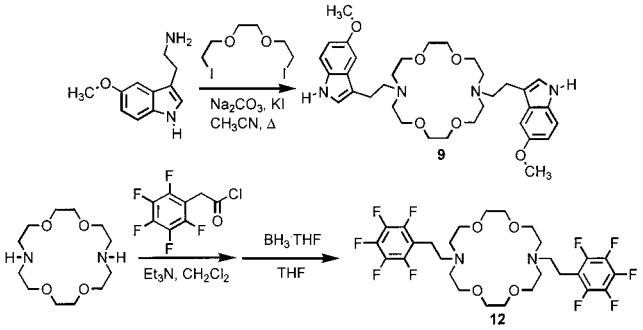

Synthetic Access. Compound **1** is commercially available and the syntheses of **2**−**5**[8] and **6**[26] were previously reported. Structures **7**−**13** were prepared either by alkylation of **1** or by using the incipient sidearm's amino group to form the macrocycle directly. Dibenzyldiaza-18-crown-6, for example, can be prepared by reaction of benzylamine with $I(CH_2CH_2O)_2CH_2$-CH_2I in the presence of K_2CO_3 and KI.[27] The approaches are shown in Scheme 1 and detailed in the Experimental Section.

Crystal Structures. All compounds were characterized by traditional chemical methods but X-ray crystallography was the main focus of the present study. Crystals of alkali metal cation complexes suitable for X-ray analysis were generally obtained by mixing equimolar amounts of alkali metal salt with the receptor in a polar organic solvent such as acetone. In some cases, crystals were obtained by slow evaporation of the solvent. In other cases, a nonpolar solvent such as diethyl ether was introduced and crystals formed by vapor diffusion. Data were collected by using either a 4-circle or CCD diffractometer. Details of crystallization, data collection, and analyses are presented in the Experimental Section.

Solid-State Conformations of Free Receptors. Solid-state structures were obtained for the free receptor molecule whenever possible. The results of X-ray diffraction studies of **7**, **10**, and **12** are shown in Figure 1. Compound **12** is the analogue of **11** in which the aromatic hydrogen atoms have been replaced by

(22) Gatto, V. J.; Arnold, K. A.; Viscariello, A. M.; Miller, S. R.; Morgan, C. R.; Gokel, G. W.*; J. Org. Chem.* **1986**, *51*, 5373−5384.

(23) Mecozzi, S.; West, A. P., Jr.; Dougherty, D. A. *J. Am. Chem. Soc.* **1996**, *118*, 2307−2308.

(24) De Wall, S. L.; Meadows, E. S.; Barbour, L. J.; Gokel, G. W. *J. Am. Chem. Soc.* **1999**, *121*, 5613−5614.

(25) De Wall, S. L.; Barbour, L. J.; Gokel, G. W. *J. Am. Chem. Soc.* **1999**, *121*, 8405−8406.

(26) Gatto, V. J.; Miller, S. R.; Gokel, G. W. *Org. Synth.* **1989**, *68*, 227−233.

(27) Gatto, V. J.; Gokel, G. W. *J. Am. Chem. Soc.* **1984**, *106*, 8240−8244.

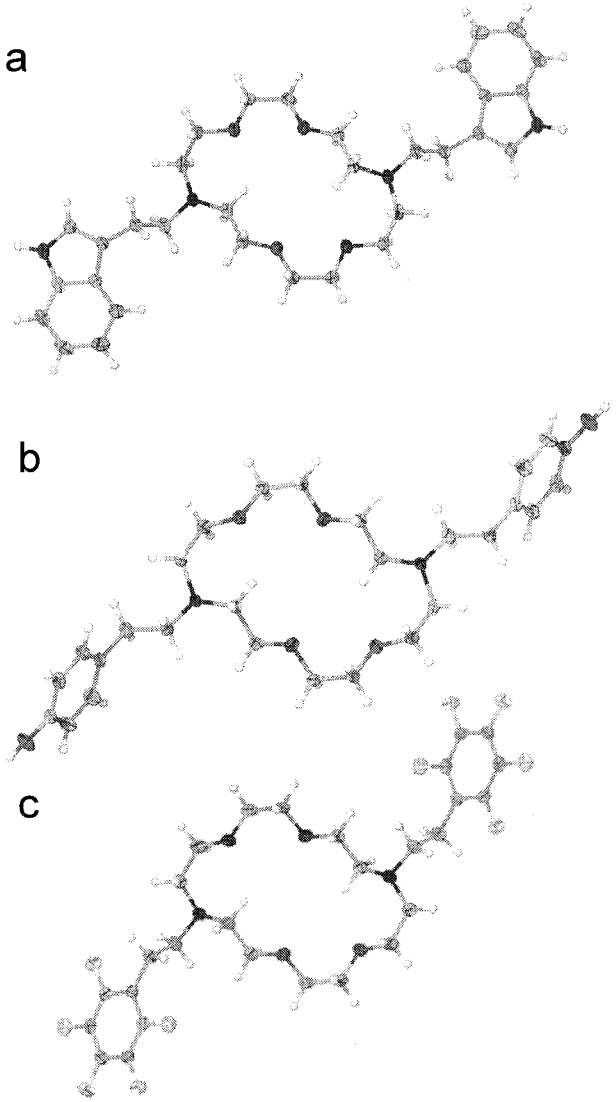

Figure 1. Conformations observed for noncomplexed **7** (a), **10** (b), and **12** (c).

fluorine atoms. Although **11** did not crystallize, compound **12** is presented here as a surrogate with the qualification that H and F are electronically different albeit similar in size. Different conformations of **7** were observed within the same crystal. Structure determinations on crystals of either **10** or **12** revealed nearly identical conformations as shown in panels b and c of Figure 1. The macroring conformations observed for these macrocycles are similar to those reported for other crowns of similar size.[28,29] Dihedral angle data for **7**, **10**, and **12** are recorded in Table 1.

Receptor 7. Two different crystal forms of receptor **7** were isolated; two independent molecules of **7** were present in the crystallographic asymmetric unit. Thus, **7** adopts at least four different solid-state conformations but the macrocycle conformation in each case was typical of diaza-18-crown-6 derivatives. Only one of these is shown in panel a of Figure 1. In all cases, the macrocycle adopts a "parallelogram arrangement" in which methylenes on opposite sides of the macrocycle rotate inward to occupy the void space. In all cases, the sidearms turn away from each other and no intramolecular interactions were noted between the sidearm and the crown for unbound **7**.

(28) Dunitz, J. D.; Seiler, P. *Acta Crystallogr. Sect. B* **1974**, *B30*, 2739−2740.

(29) Dale, J. *Isr. J. Chem.* **1980**, *20*, 3−11.

Table 1. Ethylene Dihedral Angles in the Unbound Receptors (in deg)

compd no.[a]	Crown ether ethylene units						sidearm	
7	68.3	−66.4	−175.3	−68.3	66.4	175.31	66.6	−166.6
7a[b]	62.6	71.9	−150.0	−62.6	−71.9	150.01	61.5	−161.5
7b[b]	64.2	71.6	−58.5	−52.4	−176.2	53.3	160.4	−166.2
7c[b]	62.2	69.4	−63.5	−62.2	−69.4	63.5	161.5	−161.5
10	79.5	−70.0	−178.0	−79.5	70.0	178.0	178.3	−178.3
12	73.6	−68.1	−163.7	−73.6	68.1	163.7	168.2	−168.2

[a] See Figure 1. [b] Alternative structure of **7** observed in structures not shown (see text).

The Phenol-Sidearmed Receptor, 10. The conformations of unbound phenol receptor **10** and that of **7** (Figure 1, panels b and a) are essentially identical. In both cases, the macrorings are in the "parallelogram" arrangement and all bond distances and angles are typical of that conformation. The sidearm ethylene groups are *antiperiplanar* in **10** and are oriented in approximately opposite directions extending from the macrocycle. The phenolic hydroxyl groups of **10** form intermolecular O−H···N hydrogen bonds (D_{O-N} = 2.76 Å) with adjacent molecules of **10** (not shown).

Pentafluorophenyl Receptor 12. Receptor **12** was prepared to assess the effect of reduced electron density in the arene (see below). It was expected to be structurally similar to **11** because the van der Waals radii of hydrogen and fluorine are 1.2 and 1.35 Å, respectively. Otherwise, all of the atoms in receptors **11** and **12** are identical. We assume that (if available) the structure of **11** would be similar to that obtained for **12** (Figure 1, panel c). The structure of **12** is similar to expectation and to those observed for **7** (Figure 1a) and **10** (Figure 1b). One interesting feature of noncomplexed **12** is that the fluorinated phenyl groups are involved in intermolecular edge−face π-stacking (apparent in the unit cell, not shown).

Alkali Metal Complexes of 7, 10, 11, and 12. Solid-state structures were obtained for **7**·NaI, **7**·KI, **7**·KSCN, **7**·KPF_6, **10**·NaI, **10**·KI, **11**·NaI, **11**·KI, and **12**·KI. An additional complex structure, **7**·HPF_6, was obtained that has a conformation essentially identical to that of **7**·PF_6. The K^+ complexes of **7**, **10**, and **11** exhibit similar structural features. Complexes **7**·KPF_6, **7**·NaI, **7**·KSCN, **7**·KI, **10**·KI, and **11**·KI are shown using the CPK metaphor in Figure 2, panels a and b. The structures of unbound **7** (Figure 2, panel a, middle), **7**·NaI (Figure 2, panel a, right), and **7**·KPF_6 (Figure 2, panel a, left) are shown as examples of the general structural relationship between the unbound and bound states of the synthetic receptors that form cation−π complexes.

Receptor Conformational Changes Associated with Cation Binding. In those cases in which direct comparisons can be made, i.e. **7** → **7** NaI, **7** → **7**·KI, **7** → **7**·KSCN, **7** → **7**·KPF6, **10** → **10**·KI, and (**12**) → **11**·KI, the sidearms fold back onto the macroring to make π-contacts with Na^+ or K^+ when complexation occurs. The ethylene sidearms adopt a gauche conformation as they reach above and below the mean plane of the crown. The arenes occupy the apical coordination sites of the cation and fully envelop it, excluding the counteranion, solvent, or adventitious water. In the four alkali metal complexes of **7**, the anions are H-bonded to the indole nitrogen (N1). Likewise, the phenolic hydroxyl of **10** forms an H-bond to iodide in **10**·KI.

Cation−π Sandwich Complexation of Alkali Metal Cations. The macrocycle and linkers have been deleted in the structures illustrated in Figure 2, panel c, to demonstrate the π-sandwich arrangement between the arenes and cation. Both

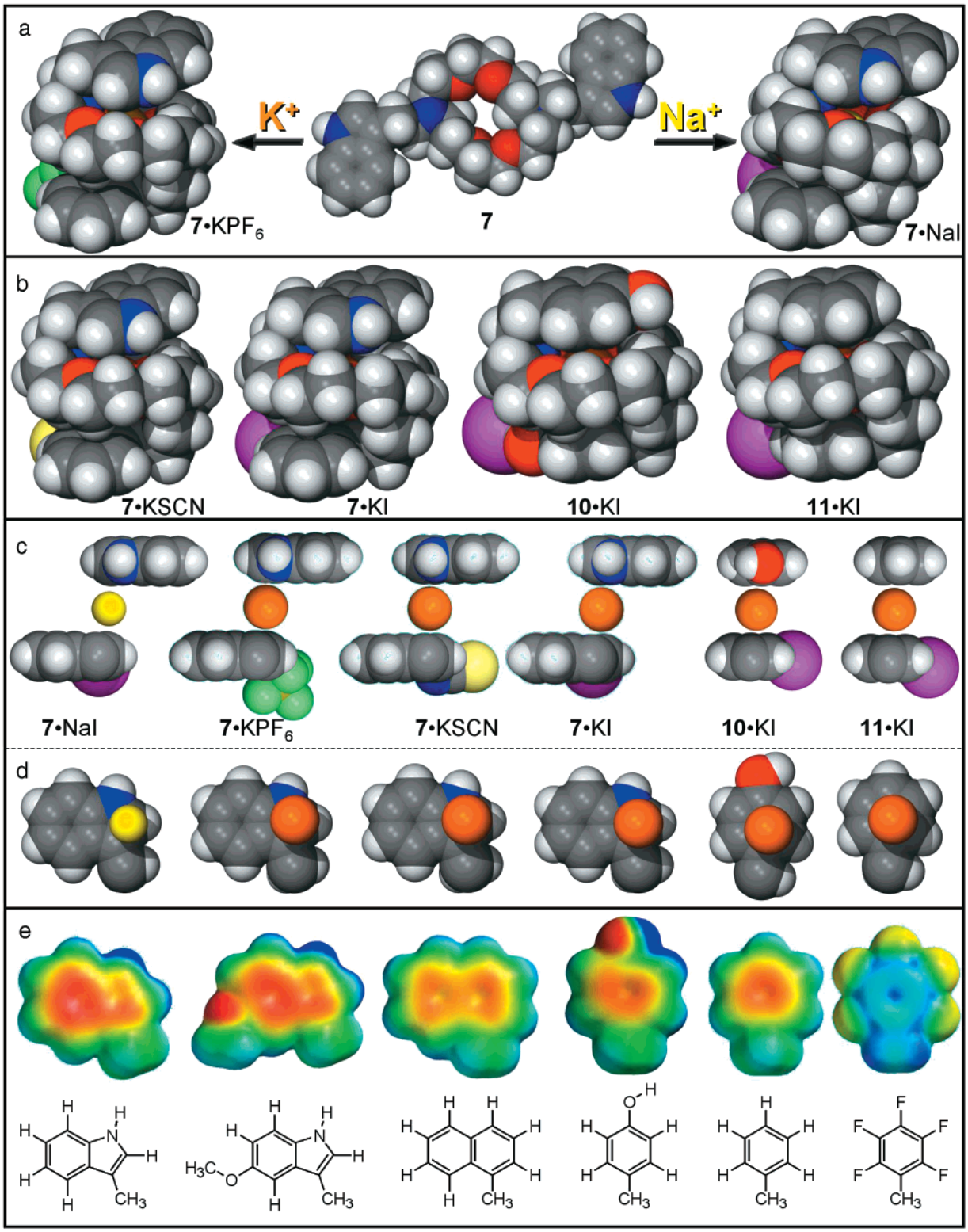

Figure 2. (a) Representations of **7** in the CPK metaphor unbound (center) and complexed by KPF_6 (left) or NaI (right). (b) Solid-state structures of the cation−π complexes **7**·KSCN, **7**·KI, **10**·KI, and **11**·KI. (c) Cross-section in the side view of arenes, cations, and anions for the complexes **7**·NaI, **7**·KPF_6, **7**·KI, **10**·KI, and **11**·KI. (d) Top and cutaway view showing the relation of the cation position to arene for the complexes shown in part c, above. (e) Electrostatic potential surfaces and chemical structures for arenes.

of the apical coordination sites of Na^+ or K^+ are fully occupied by arenes. The counterion is excluded from the coordination sphere. In all cases, the arenes on opposite sides of each cation are parallel to each other and equidistant from the cation (see Figure 2, panel c). The specific distances for each sandwich complex are shown in Table 2. Molecular interactions in the three K^+·indolyl receptor complexes (**7**·KI, **7**·KSCN, and **7**·KPF_6) are essentially identical (see below).

The distances observed for the cation−arene contacts in the solid state are 3.50 and 3.46 ± 0.03 Å for the **7**·Na^+ and **7**·K^+ complexes, respectively, and are summarized in Table 3. Ionic radii for 8-coordinate Na^+ and K^+ are reported to be 1.18 and

Table 2. Geometries of Cation−π Interactions

	distances (in Å)			angle (deg)
complex	M^+−arene	arene−arene	M^+−anion	arene−crown[a]
7·NaI	3.50	6.99	6.17	26.49
7·KI	3.45	6.89	6.06	16.48
7·KPF_6	3.48	6.95	5.48[b]	18.78
7·KSCN	3.43	6.86	5.94	17.07
10·KI	3.44	6.88	6.74	8.71
11·KI	3.43	6.86	6.56	9.18
$(\mathbf{7}\cdot 2H)^{2+}(PF_6^-)$	23.20[c]	7.02	4.72[d]	13.65

[a] Angle calculated between the macrocycle mean plane and the arene. [b] Distance from K^+ to the closest fluorine. [c] Distance from the hydrogen atom on the protonated nitrogen to the pyrrole centroid. [d] Distance from the hydrogen atom on the protonated nitrogen to the closest fluorine

Table 3. Geometry of the Cation−π Interaction Involving Indole

	M^+−R distance (Å)			
R	NaI	KI	KPF_6	KSCN
M^+-N(indole)	3.58	3.51	3.57	3.52
M^+-C2(indole)	3.23	3.32	3.30	3.38
M^+-C3(indole)	3.51	3.57	3.52	3.55
M^+-C8(indole)	4.05	3.89	3.98	3.82
M^+-C9(indole)	4.02	3.91	3.94	3.83
M^+-pyrrolo centroid	3.50	3.45	3.48	3.43
M^+-benzo centroid	4.77	4.59	4.67	4.47

1.51 Å, respectively.[30] The van der Waals radius of an aromatic carbon is reported to be 1.72−1.80 Å.[31] These values suggest an arene thickness of 3.44−3.6 Å. Using an arene thickness value of 3.5 Å, we would expect the Na^+−indole distance to be 1.75 Å + 1.18 Å = 2.93 Å. The observed Na^+−C2 distance in **7**·NaI is 3.23 Å. Thus, the separation between the Na^+ and the aromatic ring is approximately (3.23 − 2.93) = 0.30 Å on each side. For the three **7**·K^+ complexes, the corresponding K^+−C2 distances are 3.34 ± 0.04 Å. The sum of van der Waals radii for an aromatic carbon and K^+ is (1.75 + 1.51) = 3.26 Å. The separation between indole and K^+ in the **7**·K^+ complexes is therefore only about 0.1 Å.

The sidearms of **10** (ethylphenol) and **11** (ethylbenzene) correspond to the side chains of tyrosine and phenylalanine and are identical except for the presence of a hydroxyl group in the former. In each complex, the benzene ring occupies an apical position above and below the macroring to form a π-sandwich complex with K^+. The K^+ to arene centroid distances are 3.43 and 3.44 Å, respectively. The distance between the two arenes including the complexed cation (arene-arene separation) is 6.88 Å in **10**·KI and 6.86 Å in **11**·KI. Cutaway views of the **10**·K^+ and **11**·K^+ complexes are shown in panel c of Figure 2.

Position of the Na^+ and K^+ Cation with Respect to the Arene's Face in Complexes of 7, 10, and 11. The orientation of K^+ and Na^+ with respect to the indole is shown in Figure 2, panel d (four complexes of **7**). The pyrrolo, rather than the benzo, subunit serves as the π-donor in the four complexes of **7**. Indole−M^+ distances are recorded for these complexes in Table 3. In no case observed for complexes of **7** is the cation aligned exactly with either the benzo or the pyrrolo centroid. The closest contact between indole and either Na^+ or K^+ is near C2 of the indole ring. The identity of neither the cation (Na^+ or K^+) nor anion (I^-, SCN^-, or PF_6^-) alters the favored cation−π geometry with indole in these complexes of **7**.

The cation−π interaction between **7** and either Na^+ or K^+ in their respective complexes does not involve the benzene ring but rather the pyrrole subunit. The benzo ring in all of the **7**·K^+ structures is in close intramolecular contact with the C−H of an ethylene group directed toward the benzo centroid (not shown). Such C−H ···π interactions have been classified as weak "hydrogen bonds" and have received attention recently as contributing factors in molecular recognition.[32] The C−benzo centroid distance is in the range 3.79−3.88 Å in the three **7**·K^+ structures. An intermolecular C−H ···π contact is also formed in **7**·KPF_6 ($D_{C-centroid}$ = 3.88 Å) while **7**·KSCN and **7**·KI are involved in intermolecular arene−arene contacts (not shown).

Table 4. Ethylene Dihedral Angles in Lariat Ether Complexes

	dihedral angles (deg) for ethylene units in the							
	macrocyclic ring[a]						sidearm[b]	
complex	**1**	**2**	**3**	**4**	**5**	**6**	**1**	**2**
4·KBF_4	70.1	−65.8	69.0	65.2	−49.9	−55.3	n/a	n/a
5·KSCN[a]	65.8	−64.3	−50.6	−65.8	64.4	50.6	n/a	n/a
5·KSCN[b]	62.2	−21.9	63.3	−62.2	21.9	−63.3	n/a	n/a
7·NaI	59.6	−61.5	−54.6	−59.6	61.5	54.6	67.7	−67.7
7·KI	63.3	−60.7	−47.6	−63.3	60.7	47.6	62.0	−62.0
7·KPF_6	65.6	−61.1	−50.2	−65.6	61.1	50.2	64.6	−64.6
7·KSCN	63.4	−61.8	−47.3	−63.4	61.8	47.3	59.0	−59.0
$(\mathbf{7}\cdot 2H)^{2+}$-$(PF_6^-)_2$	59.2	−68.0	−48.9	−59.2	68.0	48.9	59.5	−59.5
10·KI	63.7	−59.0	−48.8	−63.7	59.0	48.8	61.4	−61.4
11·KI	62.9	−60.8	−47.9	−62.9	60.8	47.95	58.9	−58.9
12·KI	63.3	−54.1	73.2	−63.3	−73.2	54.1	176.5	−176.5

[a] Ethylene units in the macroring are consecutively numbered. [b] Ethylene units in the sidearms are arbitrarily numbered.

The cutaway top views in Figure 2, panel d, show the positions of the Na^+ and K^+ on the surface of the phenol and phenyl rings, respectively (compound numbers above structure). In **10**·KI and **11**·KI, the K^+ is positioned essentially over the center of the aromatic ring. The position of K^+ with respect to the aromatic ring is nearly identical in **10** and **11**. In both cases, K^+ is almost, but not exactly, in the center of the benzene ring.

The results of *ab initio* molecular orbital calculations are shown in panel e of Figure 2. Electrostatic potential surfaces (EPS's) were mapped onto a surface of molecular electron density and color coded for qualitative analysis. The red regions are ≤−25 kcal/mol while the blue color denotes regions of ≥+25 kcal/mol. Similar EPS's have been used to predict the calculated binding sites for Na^+ on aromatic surfaces.[19]

Macrocycle Conformation in Complexes of 7, 10, and 11. The macrocycles are slightly distorted from the expected D_{3d} conformation in **7**·NaI and the K^+ complexes of **7**, **10**, and **11**. The crown nitrogen atoms pucker slightly out of the plane and extend toward the sidearms. The dihedral angles defined by the ethylene bonds in the cation−π complexes of **7**, **10**, and **11** are shown in Table 4. For comparison, corresponding angles for dibenzyl complex **5**·KSCN and dipropargyl complex **4**·KBF_4 are also shown in Table 4. A "true" D_{3d} conformation[33] was observed for the previously reported KI complex of *N*,*N*′-bis-(2-methoxyethyl)-4,13-diaza-18-crown-6 (**14**) in which both sidearms are extensively involved in cation complexation.[34] Although there is some significant deviation (*e.g.* **7**·KSCN, **11**·KI), sidearm dihedral angles are generally near the expected

(30) Shannon, R. D. *Acta Crystallogr., Sect. A* **1976**, *A32*, 751−767.
(31) Bondi, A. *J. Phys. Chem.* **1964**, *68*, 441−451.
(32) Nishio, M.; Umezawa, Y.; Hirota, M.; Takeuchi, Y. *Tetrahedron* **1995**, *51*, 8665−701 and references therein.
(33) (a) Seiler, P.; Dobler, M.; Dunitz, J. D. *Acta Crystallogr.* **1974**, *B30*, 2744−5. (b) Dunitz, J. D.; Dobler, M.; Seiler, P.; Phizackerley, R. P. *Acta Crystallogr.* **1974**, *B30*, 2733−8. (c) Wipff, G.; Weiner, P.; Kollman, P. *J. Am. Chem. Soc.* **1982**, *104*, 3249−58.
(34) (a) White, B. D.; Fronczek, F. R.; Gandour, R. D.; Gokel, G. W. *Tetrahedron Lett.* **1987**, *28*, 1753. (b) Gandour, R. D.; Fronczek, F. R.; Gatto, V. J.; Minganti, C.; Schultz, R. A.; White, B. D.; Arnold, K. A.; Mazzochi, D.; Miller, S. R.; Gokel, G. W. *J. Am. Chem. Soc.* **1986**, *108*, 4078.

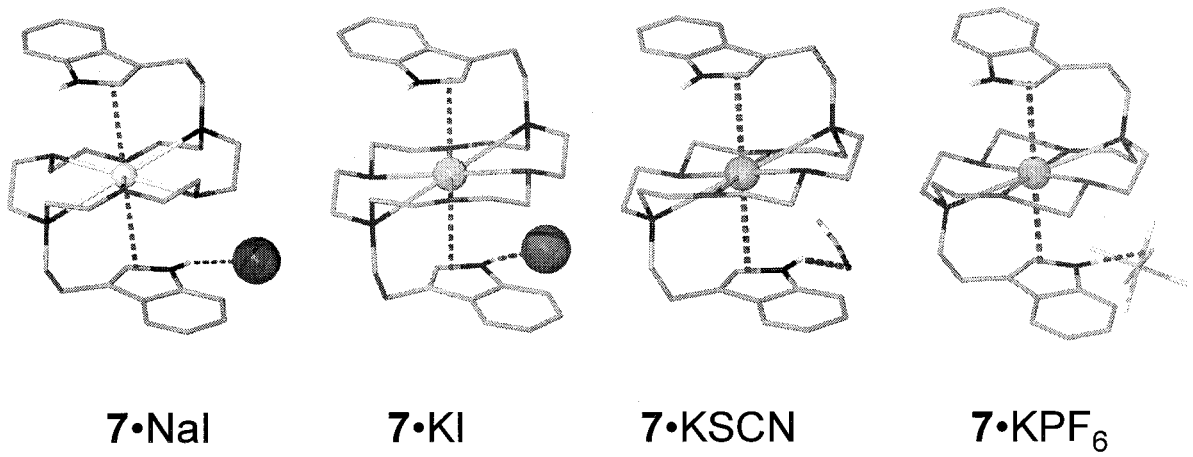

Figure 3. Structures of **7**·NaI, **7**·KI, **7**·KSCN, and **7**·KPF_6 shown in the tube metaphor. Dotted lines indicate cation$-\pi$ and H-bond contacts.

value of 60°. The homology between the complexes of **7**, **10**, and **11** is apparent from the fact that the standard deviations observed for each of the macroring dihedral angles is <3 (data shown in Table 4).

Although the macrocycles in the cation$-\pi$ complexes of **7**, **10**, and **11** are not in a precise D_{3d} arrangement, the distances between the donor atoms and the cations are typical. For example, the K^+-O distances for the **7**·K^+ complexes are in the range 2.75 ± 0.1 Å. The K^+-N distances are 3.02 ± 0.05 Å. The corresponding distances for **14**·KI (macroring in D_{3d} conformation) are as follows: $K^+-O = 2.83 \pm 0.03$ Å, $K^+-N = 2.94$ Å. Thus, the bond distances are typical for alkali metal complexes of 18-membered crowns. In complexes exhibiting a cation$-\pi$ interaction with the arene, the ethylene unit in the sidearm adopts a *gauche* conformation (see Table 4). In the phenyl-terminated sidearm complexes, K^+ is also positioned near the center of the macroring. In both **10**·KI and **11**·KI, the macrocycle adopts a distorted D_{3d} conformation and the K^+-O (2.68−2.70 Å) and K^+-N distances (3.04−3.06 Å) are as expected.

Differences in the Alkali Metal Cation Complexes. Despite the numerous similarities in overall conformation in the structures discussed above, there are several notable differences. The unique features of each cation$-\pi$ complex are described below. Throughout this section, tube representations of each structure are shown individually. Dashed lines in each figure connect the cation with the aromatic group to show the bonding axis between the π-system and the cation.

Structures of 7·NaI, 7·KI, 7·KSCN, and 7·KPF_6. The similarity in these four structures is apparent from Figure 3. Several features are notable. First, the macrocyclic rings are in the expected conformation although they are somewhat distorted from D_{3d}. For the most part, the bond angles and distances are typical. The N−N distance across the crowns is about 6.1 Å in these four **7**·M^+ complexes. Typically, the M^+-O distances are shorter than the M^+-N distances. Typical values are $Na^+-O = 2.47 \pm 0.01$ Å and $Na^+-N = 3.03$ Å for **7**·NaI. The corresponding K^+-O and K^+-N distances in **7**·KI are 2.70 ± 0.06 and 3.06 Å, respectively. The dihedral angles (see Table 4) for the ethylene units in the crown are all near ±60°, although variations to ∼55° are observed.

The most interesting feature of **7**·NaI is the cation$-\pi$ interaction between the indole groups and Na^+. The **7**·NaI complex is the only example we have obtained of a cation$-\pi$ interaction involving Na^+. This is surprising in light of the experimental measurements[3,35] in the gas phase that have demonstrated the much stronger binding energy for benzene·Na^+ compared to benzene·K^+ ($\Delta H = -28.0$ and −18.3 kcal/mol, respectively, see below). Calculations have also found that the attraction is greater between benzene and the smaller, more charge dense, Na^+ compared to the larger K^+.[36]

In **7**·NaI, the distance between the centroids of the pyrrolo fragments of the indole group is 6.99 Å. The iodide ion shown in Figure 3 is excluded from the first solvation sphere of the cation ($Na^+-I^- = 7.16$ Å) but H-bonded to the indole nitrogen (N1). In **7**·NaI, the arene is tilted 26.49° with respect to the mean plane of the macrocycle. The tilting of the indole ring is greater in **7**·NaI than in any of the other cation$-\pi$ complexes. The angle between the crown and the arene results in the shortest Na^+-C2 distance observed (see Table 3). The angle between the crown and the indole ring is 16.48°, about 10° less tilted than in **7**·NaI, reflecting this difference. In **7**·KPF_6, the indole ring is canted by 18.78° with respect to the macrocycle's mean plane; this value is similar to that observed for **7**·KI. The angle between the macrocycle mean plane and the indole ring in **7**·KSCN is 17.07°.

In all four cases, the counteranion is hydrogen bonded to the indole nitrogen. Unlike the iodide ion, the thiocyanate ion in **7**·KSCN is disordered. This contrasts with the KSCN complex of *N*,*N*′-bis(benzyl)-4,13-diaza-18-crown-6, **5**, in which the thiocyanate anion occupies the apical coordination sites of the bound potassium cation.[37]

Structures of 10·KI and 11·KI. The macrorings in **10**·KI and **11**·KI are nearly planar but slightly distorted from the D_{3d} conformation (see Figure 4). Heteroatom to cation distances are as expected. The phenolic hydroxyl group is hydrogen bonded to the iodide anion. The O−H···I hydrogen bond angle is 170.5°. The phenolic benzene ring is positioned nearly parallel to the macrocycle's mean plane; the two planes intersect at an angle of 8.71° in **10**·KI and 9.18° in **11**·KI. The "centerline" distance between the two aromatic centroids is 6.87 ± 0.01 Å and the cation is positioned between them at their midpoint. Unlike **10**·KI, there is no group available to H-bond to iodide in **11**·KI. The iodide anion is positioned approximately coplanar with the cation and macroring but excluded from the solvation sphere.

(35) Guo, B. C.; Purnell, J. W.; Castleman, A. W., Jr. *Chem. Phys. Lett.* **1990**, *168*, 155−160.
(36) Caldwell, J. W.; Kollman, P. A. *J. Am. Chem. Soc.* **1995**, *117*, 4177−4178.
(37) Arnold, K. A.; Viscariello, A. M.; Kim, M.; Gandour, R. D.; Fronczek, F. R.; Gokel, G. W. *Tetrahedron Lett.* **1988**, *29*, 3025−8.

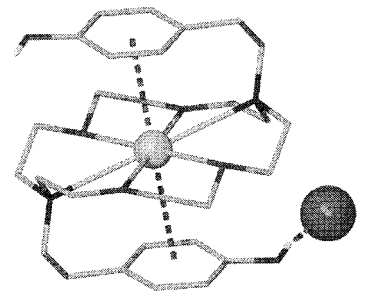

10·KI

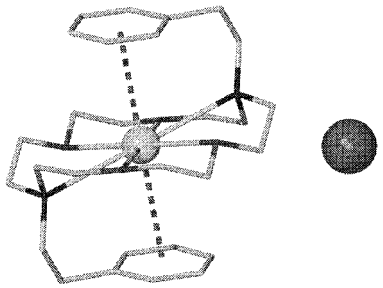

11·KI

Figure 4. Structures of **10**·KI and **11**·KI shown in the tube metaphor. Dotted lines indicate cation−π and H-bond contacts.

Structures of $(7\cdot 2H)^{2+}(PF_6^-)_2$, $7\cdot NaPF_6$, and 9·NaI. The three complexes shown in Figure 5 have unusual aspects. Diprotonated **7** is similar to **7**·KPF_6 although no alkali metal cation is present. The two macroring NH bonds point toward the center of the macroring. One of the PF_6^- counterions is H-bonded to the indole NH, which makes contact with the edges of the aromatic rings (not shown). The sidearms of $(7\cdot 2H)^{2+}(PF_6^-)_2$ are positioned above and below the positively charged crown and the angle between the mean plane of the macrocycle and either arene is 13.65°. The pyrrolo centroids are separated by 7.02 Å.

Like the other PF_6^- complexes in this study, the anion in **7**·$NaPF_6$ is H-bonded to indole. The indole rings, however, do not π-complex Na^+. The macroring is contracted; the transannular N−N distance is 4.96 Å compared to >6 Å in other complexes. Likewise, compound **9** does not form a $Na^+-\pi$ complex in the solid state. Instead, the indole rings contact the iodide ion through N−H···I^- hydrogen bonds (d_{N-I} = 3.89, 3.57 Å). The macroring N−N separation in **9**·NaI is 4.42 Å. A water molecule bridges two crown·Na^+ units to form a head-to-head dimer (not shown).

Structure of 10·NaI. The structures of **10**·NaI and **11**·NaI are generally similar. In both cases, the crystallographic asymmetric unit contains two unique but similar molecules. Because the two complexes are quite similar, only one of the **10**·NaI complexes is shown in Figure 6. The macrocycle in **10**·NaI adopts an overall saddle-like shape, arranging the π-donors three-dimensionally rather than in a plane. The six macroring heteroatoms (Z) are organized around bound Na^+ in a distorted octahedral geometry. The Z−Na−Z angles (70.1 ± 4.4°) are intermediate between 60°, expected for a planar structure, and 90° (octahedral). Five of the O−C−Z angles are ∼69° but the sixth is 74.6°, causing the deviation. The N−Na−N angle is 122.2° rather than 180° as expected for a nearly planar, D_{3d} macroring conformation. The two Na−N distances are 2.52 and 2.60 Å. The Na^+−O distances are 2.35, 2.35, 2.38, and 2.47 Å. The sidearms in **10**·NaI extend upward, with the phenolic residues contacting I^- at the apex of the structure. The two phenolic oxygen atoms are about equidistant from iodide ($D_{O\cdots I}$ = 3.46 and 3.47 Å).

Structure of 11·NaI. In **11**·NaI, the cation is bound by the macroring but not by the sidearms. The solid-state structure of **11**·NaI (Figure 6) is similar to that of **10**·NaI and **5**·NaI. In each case the macrocycle is puckered to more fully immerse the cation in the macroring while the two sidearms extend upward. There are six disordered water molecules present in the asymmetric unit of **11**·NaI; the Na^+ cation is coordinated by only one of them. Hydrogens could not be accurately placed on the disordered water oxygen atoms but it appears that the I^- counterion is close enough to form an I···H−O hydrogen bond to the Na^+-coordinated water (3.67 and 3.78 Å). The Na^+ cation in **11**·NaI is 7-coordinate and the Z−Na−Z angles are 67.9 ± 0.8°. The sidearm donor groups are positioned on the same side of the macroring (syn) rather than anti as in the π-coordinated complexes of **7**, **10**, and **11**.

Structure of 12·KI. The solid-state structure of **12**·KI (Figure 7) revealed no sidearm coordination of the ring-bound K^+ ion although the macroring conformation is similar to that of **11**·KI. The K^+ to oxygen and to nitrogen distances are also similar to those of **11**·K^+. The sidearm ethylene groups are both in the *antiperiplanar* (176.5°) conformation in **12**·K^+. Because neither arene in **12**·K^+ is involved in π-complexation, the K^+ ion is accessible to the I^- counterion. Each iodide thus bridges two molecules of **12**·K^+ to form an extended, linear $(K^+\cdots I^-)_n$ network.

Structures of 13·KI and $13\cdot KPF_6$. Neither **13**·K^+ exhibits cation−π complexation; the ring ethylenes are approximately *gauche*. In both cases, the K^+ ion is coordinated by the six crown ether donor groups (K^+−O = 2.77 Å, K^+−N = 3.08 Å) that lie in a plane surrounding the cation (shown at the right of Figure 7). The apical positions are occupied by I^-, which also contacts a neighboring K^+ to form a columnar $(K^+\cdots I^-)_n$ network as observed for **12**·KI. The naphthyl residues are oriented away from the macrocycle (anti orientation of the sidearm ethylene units). The naphthalenes form intermolecular edge-face contacts with an adjacent **13**·KI complex. The disordered $-CH_2CH_2-$ naphthyl groups in one molecule of **13**·KI were successfully modeled ($R1$ = 7.6%) to occupy two positions, each with half occupancy. One of the two positions is shown as an ellipsoid plot while the other is represented by the dotted lines (see Figure 7). Crystals of **13**·KPF_6 were disordered but were found to be isostructural with **13**·KI. The structure was solved only to the extent that the conformation of the crown and the orientation of the sidearms were apparent.

Solution NMR Studies: NOESY Data for 7. 2D NOESY experiments were conducted on **7** in CD_3COCD_3 in the absence and presence of NaI. The solution data suggest a structure in accord with that observed for the solid state. Figure 8 shows the solid-state structure along with superimposed arrows that indicate NOE cross-peaks. In the absence of salt (broken arrows), strong NOE cross-peaks are observed between the resonance due to unresolved spacer arm hydrogens and indole's H2 and H4 hydrogens (see Figure 16 for numbering). Other NOEs are also observed in accord with the proposed structure, but the cross-peaks of the indole H2 and H4 atoms with the crown hydrogens are the most significant peaks involving crown−sidearm interactions.

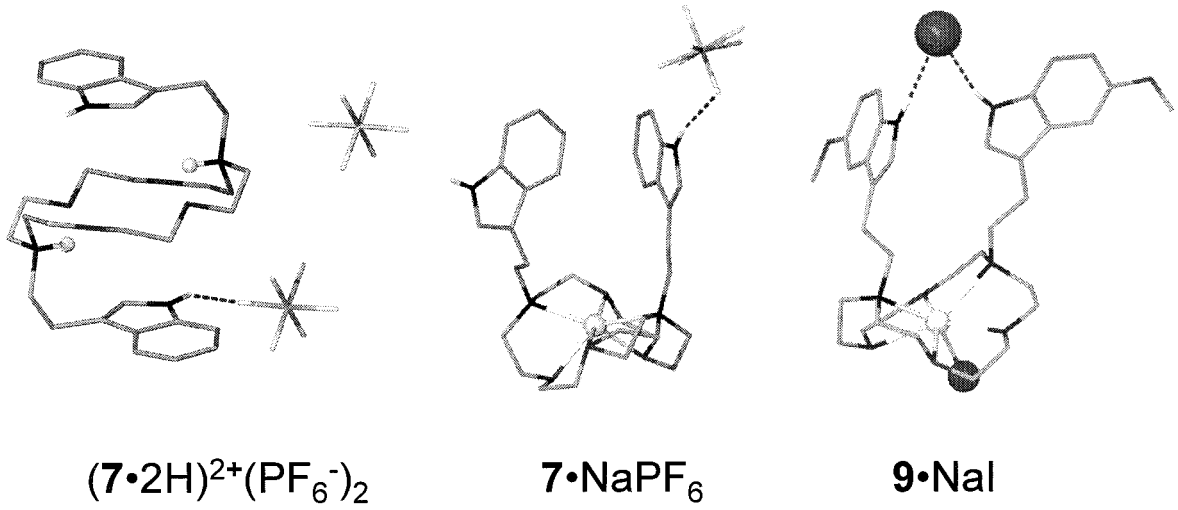

Figure 5. Structures of **7**·$H_2(PF_6)_2$, **7**·$NaPF_6$, and **9**·NaI shown in the tube metaphor. Dotted lines indicate H-bond contact.

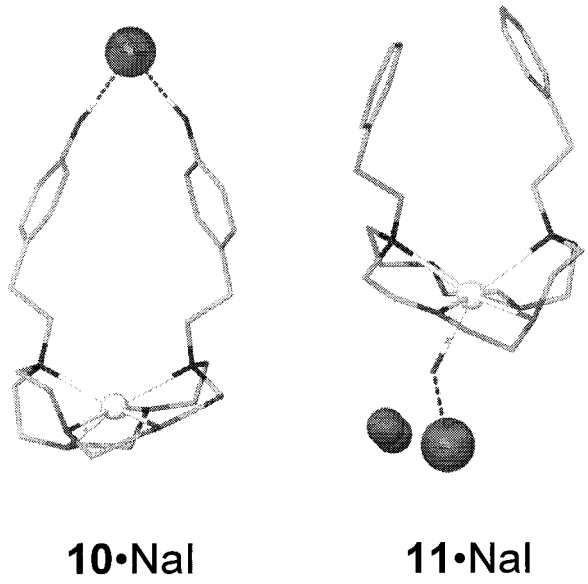

Figure 6. Structures of **10**·NaI and **11**·NaI $(H_2O)_2$ shown in the tube metaphor. Dotted lines indicate H-bond contacts.

When NaI is added, the cross-peak between the indole H4 and the crown hydrogens disappears. Cross-peaks were observed between H2 and both Hc and the side chain methylenes in the complex. New cross-peaks between H7 and both Hb and Hc were observed in the complex (solid arrows in Figure 8). Thus the structure inferred by the 2D NOESY data comports with the solid-state result.

Titration of 7 and 8 with NaI. The side chains of **7** are terminated by indoles attached at the 3-position. Compound **8** is identical except that the indole nitrogen atom (1-position) is methylated. In separate experiments, each compound (5 mM in CD_3COCD_3) was titrated with NaI (0.5 M in CD_3COCD_3) at room temperature. Chemical shift changes were assessed by ^{1}H NMR and the results are graphed in Figure 9. For **7**, the largest observed chemical shift increment was for H2 (▲): $\Delta\delta_\infty = -0.30$ ppm.This was expected because H2 was closer to the bound cation than was any other hydrogen atom in every solid-state complex of **7** obtained thus far (**7**·NaI, **7**·KI, **7**·KSCN, and **7**·KPF_6). The macroring hydrogens of **7** [H_a (Δ), H_b (∇)] showed typical downfield shifts upon complexation. The hydrogen on the indole nitrogen [H1 (■)] was also shifted downfield to a comparable degree. Hydrogens on the benzo portion of the indole (H4−H7) exhibited modest shifts (=0.10 ppm). The latter chemical shifts are expected to be relatively unaffected by complexation because the solid-state structures show that they are most remote from the cation.

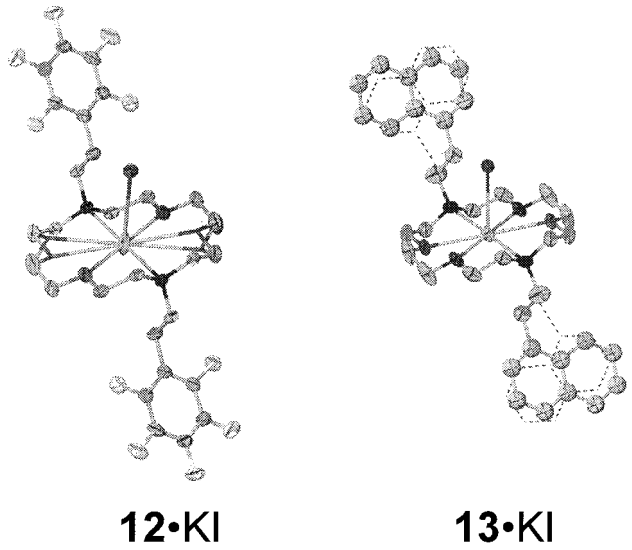

Figure 7. Structures of **12**·KI and **13**·KI shown in an ORTEP plot.

The ^{1}H NMR chemical shift changes observed when **8** was titrated as above with NaI corresponded to those observed for **7** but were generally more modest. The largest chemical shift increments were ±0.2 ppm (H_a, H2) rather than nearly −0.3. The protons most affected in **8** were the same as those in **7** and the magnitudes of the chemical shift changes are more similar than different for the two systems. We therefore conclude that a similar conformation is present in both cases but this is verified for the solid state only in the case of **7**.

Discussion

Indole as a π-Donor. Tryptophan has a 2-(3-indolylethyl) side chain and can be categorized as either hydrophobic or hydrophilic depending on the solvent system employed in the study,[41] but in either case, it possesses a π-system. The positively

(38) Meadows, E. S.; De Wall, S. L.; Barbour, L. J.; Gokel, G. W. *Chem. Commun.* **1999**, *16*, 1555−1556.
(39) De Wall, S. L.; Meadows, E. S.; Barbour, L. J.; Gokel, G. W. *Proc. Natl. Acad. Sci. U.S.A.* **2000**, *97*, 6271−6276.
(40) Live, D.; Chan, S. I. *J. Am. Chem. Soc.* **1976**, *98*, 3769−3778.

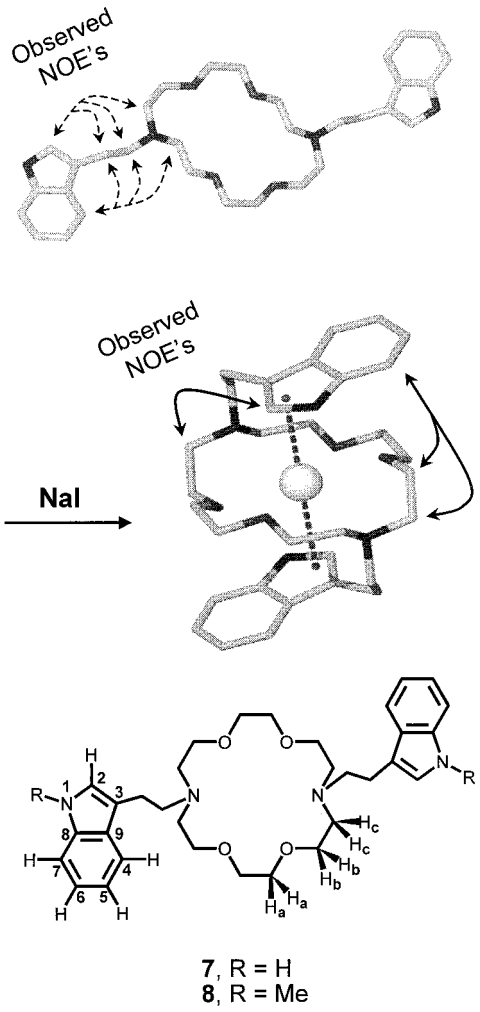

Figure 8. The solid-state structure of unbound and sodium-complexed **7** shown with the chemical structures of **7** and **8**. Dashed and solid arrows indicate ^{1}H NOE's observed in Me_2CO solution.

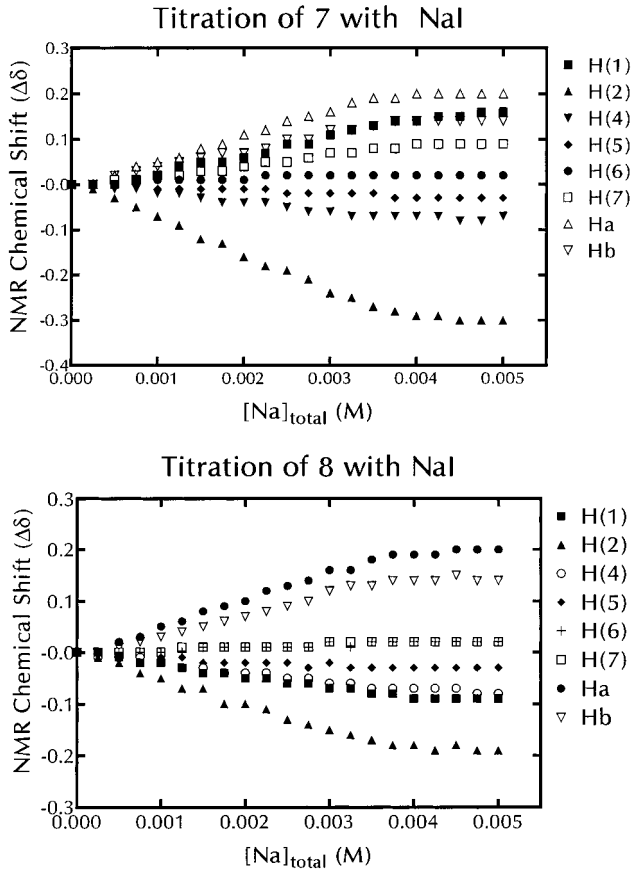

Figure 9. Graph showing ^{1}H NMR shifts resulting from titration of **7** (top) or **8** with NaI in CD_3COCD_3.

polarized hydrogens of water may interact with the π-surface of indole or benzene. Indole has recently been shown by gas-phase calculations to bind water to its π-surface by formation of "π-type hydrogen bonds" almost as well as by traditional $N_{indole}-H\cdots O_{water}$ hydrogen bonds.[42] A report by Atwood and co-workers demonstrated experimentally the existence of an $O-H_{water}$ π hydrogen bond.[43] Recent gas-phase measurements have confirmed the surprisingly strong attraction between water and benzene.[44] In these cases, the water hydrogens were directed toward the benzene centroid as expected for a cation−π interaction.

Although calculations showed that the benzo ring is the preferred π-donor in indole, Whipple and co-workers reported in 1962 that indole is protonated preferentially at either C2 or C3 (pyrrolo subunit) depending upon indole's substitution pattern.[45] Experimental examples in the recent literature suggest that either the benzo or the pyrrolo subunit can coordinate cationic species. Aoki and co-workers observed both inter- and intramolecular quaternary ammonium ion−π interactions involving the choline ester of 3-indolylacetic acid.[46] The closest (3.36 Å) contact was between Me_3N^+ and the pyrrolo ring of an adjacent indole. A further example, found in a search of the Protein Data Bank (PDB),[47] illustrates a bifurcated cation−π interaction in the active site of acetylcholine esterase. One of the carbons from decamethonium (a quaternary amine inhibitor) is within 4.0 Å of the benzo subunit and another carbon is 4.0 Å from the pyrrolo centroid. A similar interaction was observed in the phosphocholine complex of the antibody fragment McPC603.[48] We also note that a search of the Cambridge Structural Database (CSD)[49] for small molecule crystal structures and a previous study by Verdonk *et al.*[50] provide evidence of ammonium−benzene interactions. A limited amount of solid-state structural evidence for cation−π interactions has been available for a number of years although many examples have not been well recognized. An important example is the report by Atwood and co-workers of a dibenzo-18-crown-6·K^+

(41) (a) Radzicka, A.; Wolfenden, R. *Biochemistry* **1988**, *27*, 1664−70. (b)Wolfenden, R.; Radzicka, A. *Trends Biochem. Sci.* **1986**, *11*, 69−70.

(42) (a) Mons, M.; Dimicoli, I.; Tardivel, B.; Piuzzi, F.; Brenner, V.; Millie, P. *J. Phys. Chem. A* **1999**, *103*, 9958−9965. (b) Carney, J. R.; Zwier, T. S. *J. Phys. Chem. A* **1999**, *103*, 9943−9957.

(43) Atwood, J. L.; Hamada, F.; Robinson, K. D.; Orr, G. W.; Vincent, R. L. *Nature* **1991**, *349*, 683−4.

(44) (a) Rodham, D. A.; Suzuki, S.; Suenram, R. D.; Lovas, F. J.; Dasgupta, S.; Goddard, W. A., III; Blake, G. A. *Nature* **1993**, *362*, 735−7. (b) Suzuki, S.; Green, P. G.; Bumgarner, R. E.; Dasgupta, S.; Goddard, W. A., III; Blake, G. A. *Science* **1992**, *257*, 942−5. (c) Zwier, T. S. *Annu. Rev. Phys. Chem.* **1996**, *47*, 205−241.

(45) Hinman, R. L.; Whipple, E. B. *J. Am. Chem. Soc.* **1962**, *84*, 2534−2539.

(46) Aoki, K.; Maruyama, K.; Nishiyama, H. J. C. S. *Chem. Commun.* **1995**, 2221−2222.

(47) (a) Berman, H. M.; Westbrook, J.; Feng, Z.; Gilliland, G.; Bhat, T. N.; Weissig, H.; Shindyalov, I. N.; Bourne, P. E. *Nucleic Acid. Res.* **2000**, *28*, 235−242. (b) Bernstein, F. C.; Koetzle, T. F.; Williams, G. J. B.; Meyer, E. F., Jr.; Brice, M. D.; Rodgers, J. R. K.; Olga; Shimanouchi, T.; Tasumi, M. *J. Mol. Biol.* **1977**, *112*, 535−42.

(48) Satow, Y.; Cohen, G. H.; Padlan, E. A.; Davies, D. R. *J. Mol. Biol.* **1986**, *190*, 593−604.

(49) (a) Kennard, O. *Supramol. Chem.* **1993**, *1*, 277−95. (b) Allen, F. H.; Kennard, O.; Taylor, R. *Acc. Chem. Res.* **1983**, *16*, 146−53.

(50) Verdonk, M. L.; Boks, G. J.; Kooijman, H.; Kanters, J. A.; Kroon, J. J. *Comput.-Aid. Mol. Des.* **1993**, *7*, 173−82.

complex in which benzene solvent occupied an apical donor site.[7b] In the present work, we set as a goal the systematic assessment of alkali metal cation−π interactions with benzene, phenol, and indole, the side chains of the aromatic amino acids Phe, Tyr, and Trp.

Artificial Receptors as Biological Model Systems. The receptor molecules used in the present studies are neither peptides nor proteins but possess advantages over both. Receptors **1**−**13** and their complexes all have molecular weights of ≤850 Da. For molecules of this size, typical crystals diffract well enough to afford resolutions better than 0.8 Å. Thus, the atomic positions and parameters (bond lengths, bond angles, etc.) are extremely well determined. This is a significant advantage compared to protein structures, for which the resolution is often only 2−3 Å. In addition, the receptor systems were designed to be closely related to each other. The arene in each case is covalently attached to the macrocycle in an orientation and at a distance appropriate to permit a cation−π interaction, eliminating the need for providential contacts. As only the receptor side chains and salts are varied in the receptors used in this study, we can directly compare the resulting complex structures.

A peptide containing 30 amino acids will have a molecular weight[51] of 3−4000 Da. A protein of only 200 amino acids will have a molecular weight of more than 20 kDa. Like the crystal structure determinations, solution and computational studies are easier using these lower molecular weight model systems than for peptides or proteins.

Sodium and Potassium Complexes of 7. The Na^+ and K^+ complexes of **7** comprise the first experimental documentation of Na^+ and K^+ cation−π sandwich interactions of indole. It is clear from CPK molecular models that π-coordination of a ring-bound cation in **7** could involve either the benzo or the pyrrolo subcyclic units. Several theoretical calculations have been reported for alkali metal cation−π complexation[4,5,13] and, in all cases, the benzo residue is predicted to coordinate the cation. To our knowledge, no previous small molecule X-ray structure of a complex involving a direct interaction between indole and either Na^+ or K^+ has been reported. Wouters has recently reported a Na^+−tryptophan contact in the structure of lysozyme but the distance reported for the arene−cation contact is >4 Å.[52] An intriguing example of a Cs^+−Trp interaction was reported by Hol and co-workers in the crystal structure of rhodanese.[53] In this case, the cesium cation is clearly coordinated by the benzo ring of the indole side chain.

In contrast to theoretical predictions, it is the pyrrolo, rather than the benzo, subcyclic unit that coordinates with the alkali metal in **7**·NaI and **7**·KI. The preference of pyrrolo as a donor for either Na^+ or K^+ in complexes of **7** is independent of the counterion. Indeed, the solid-state structures of **7**·KI, **7**·KSCN, and **7**·KPF_6 are essentially superimposable, exclusive of the anion. In all cases studied (**7**·NaI, **7**·KI, **7**·KSCN, and **7**·KPF_6) in which cation−π complexation is observed, the anion is excluded from the cation's coordination sphere and is at a distance from the cation of at least 5.4 Å.

Solution Studies of 7 and 8. The interaction of sodium cation with receptors **7** and **8** was assessed in two different ways. First, the NOESY spectrum for **7** was obtained in CD_3COCD_3 solution. The cross-peaks observed suggested proximity between C2 and C4 on the sidearm indoles and the adjacent macrocycle. These interactions are expected for a conformation of **7** in which the sidearms are extended from the macrocycle. When NaI was added, the cross-peaks involving C4 hydrogens were no longer observed. Instead, new peaks suggested that C2 was close to one side of the macroring and C7 was close to the opposite side. These interactions suggest a solution conformation consistent with that observed in the solid state (Figure 3).

The effect of NaI complexation on the ^1H NMR spectra of **7** and **8** was also assessed. Addition of NaI (0 to 1 equiv) caused a continuous alteration in the chemical shifts. It seemed possible that the solution conformation was being controlled by H-bond formation between the anion or solvent and the indole nitrogen. Replacement of the 1-hydrogen with a methyl group afforded **8**. The observed chemical shift differences were smaller for **8** than for **7** but the trends were similar. Moreover, C2 remained the most shifted aromatic resonance in **8**, as was the case for **7**.

A Non-π-complexed Conformation for 7·$NaPF_6$. The K^+ complexes of **7** that exhibit cation−π interactions are generally similar. They are also similar to **7**·NaI, in which cation−π interactions are also observed. In contrast, the solid-state structure of **7**·$NaPF_6$ is very different from that observed for **7**·$NaPF_6$ and **7**·KPF_6 (see Figure 5) particularly with respect to the orientation of indole-terminated sidearms. For the cation−π complexes, the sidearm ethylene adopts a *gauche* arrangement such that the indole rings of **7** form a tight cation−π sandwich complex with K^+. In contrast, the sidearms in **7**·$NaPF_6$ adopt the *antiperiplanar* arrangement.

The non-π-conformation adopted by **7**·$NaPF_6$ represents an energy minimum but its relative stability in solution compared to other conformations is unknown. One interesting observation is that the Na^+−O distances in **7**·NaI and **7**·$NaPF_6$ are nearly the same but the Na^+−N distances in the latter are significantly shorter. This suggests a greater cation coordination role for the nitrogen donors and thus the macroring. Presumably, this increased π-donation compensates for the absence of π-interactions. The more contracted ring in the non-π complex may also force the sidearms into the "tent" arrangement apparent in Figure 5. The difference in conformation between **7**·NaI and **7**·$NaPF_6$ cannot be attributed solely to the difference in counteranion since both I^- and PF_6^- are excluded from the solvation sphere. Moreover, **7**·KPF_6 forms a cation−π complex.

A Dicationic Structure Having a π-Complexed Conformation. One of the most intriguing complexes studied in the effort reported here was $(\mathbf{7}\cdot 2H)^{2+}(PF_6^-)_2$. It was thought that we might obtain an ammonium ion−π complex by treating **7** with NH_4^+. Evidently, proton transfer from NH_4^+ to the macroring nitrogens of **7** occurred, affording diprotonated **7** $(\mathbf{7}\cdot 2H)^{2+}$. A combination of low-temperature X-ray analysis and high-quality crystals allowed for the two protons to be located on the crown nitrogen atoms. The proton positions were assigned based on the geometry of the macrocycle and the observation of electron density in the obvious protonation sites.

Although no metal ion is present in the macroring, the structure parallels those found for **7** M^+ complexes in which cation−π interactions are observed. The sidearms in $(\mathbf{7}\cdot 2H)^{2+}(PF_6^-)_2$ are organized above and below the macroring plane as if solvating the void in the center of the crown. The overall compactness of this structure may be important in determining the sidearm positions. Ammonium ion π-complexation of the type that may occur in this system has been the subject of theoretical studies[54] and is known in protein structures.[55]

Receptors 8 and 9: Variations in the Indole Side Chains of 7. The *N*-methylindole receptor, **8**, was prepared to probe the effect of preventing the indole group from H-bonding.

(51) Calculation based on a weighted average molecular weight for an amino acid of 119.

(52) Wouters, J. *Protein Sci.* **1998**, *7*, 2472−2477.

(53) Kooystra, P. J. U.; Kalk, K. H.; Hol, W. G. J. *Eur. J. Biochem.* **1988**, *177*, 345−349.

Unfortunately, no solid-state structure was obtained for **8**·M^+. The solution data described above, however, suggest that similar interactions occur when either **7** or **8** is titrated with NaI. Thus, the potential H-bonding role of the indolyl NH may be unimportant in determining the conformations of the receptor complexes.

The binding energies of Na^+·5-methylindole (33.4 kcal/mol) and Na^+·5-aminoindole (36.4 kcal/mol) have been calculated to be greater than that for Na^+ indole (32.6 kcal/mol). Despite the presence of the electron-donating methoxy group, the electrostatic potential surfaces of 5-methoxy-3-methylindole and 3-methylindole are qualitatively similar (Figure 2, panel e). A quantum mechanical calculation (see the Experimental Section) of the Na^+·5-methoxyindole complex gave a binding energy of 34.1 kcal/mol, about 5% greater than that of indole. The similarity in calculated binding energies suggests that it is not differences in π-donicity that prevent complex formation, but the data are otherwise unrevealing. Based on π-donicity alone, **9** should form an indole sandwich complex with NaI, as was the case for **7**. Clearly, steric factors may play a role in this case, but our inability to obtain crystals of a complex of **9** + NaI does not constitute evidence.

Phenol- and Benzene-Sidearmed Complexes, 10·MI and 11·MI. The solid-state structures of **10**·KI and **11**·KI are similar (see Results). In both cases, the macroring adopts a distorted D_{3d} conformation, the apical coordination sites are filled by the arenes, and the iodide ion is excluded from the cation's coordination sphere. In **10**·K^+, the phenolic hydroxyl group is H-bonded to iodide, but in **11**·K^+, no hydrogen bond donor is accessible to the iodide counterion. In both cases, the center of the arene is aligned with the cation in accord with theoretical predictions. The position of the cations relative to the arenes in **10**·KI and **11**·KI agrees with the electrostatic potential surface calculated for 4-methylphenol and 4-methylbenzene shown in panel e of Figure 2.

Similar conformations are observed for **10**·NaI and **11**·NaI, but in neither case do the sidearms coordinate the cation. The sidearms of both complexes are extended upward from the approximate plane of the macroring. The phenolic hydroxyls of **10** H-bond to iodide in the NaI complex. This is not possible for **11**·NaI but the sidearms exhibit a similar arrangement. Iodide anion is H-bonded in **11**·NaI but to a water molecule that is bound to Na^+ within the macrocycle.

The difference in conformation observed between Na^+ and K^+ complexes for receptors **10** (ethylphenol sidearm) and **11** (ethylbenzene sidearm) is noteworthy. In principle, Na^+, which is more charge dense, should be more strongly complexed by a π-donor than K^+. This has been confirmed experimentally for benzene with Na^+ and K^+ (gas phase, difference in binding energy is 8.8 kcal/mol),[5,35] and phenol is anticipated to behave similarly. Although essentially featureless spheres, Na^+ and K^+ differ in size (2.36 Å vs 3.02 Å for the 8-coordinate cations).[30] Since no cation−π interaction is observed between Na^+ and **10** or **11**, we surmise that the difference in steric interactions, in particular the thickness of the macrocycle relative to the sizes of Na^+ and K^+, prevents the observation of a Na^+−arene interaction in these two model systems.

Molecular models suggest that the aromatic rings of the phenol (**10**) and phenyl (**11**) receptors cannot penetrate deeply enough into the macroring's cavity to coordinate Na^+. The larger size of K^+ diminishes the role of steric interactions in this complex. The K^+ cation (radius = 1.51 Å) is a better fit for the 18-membered macrocycle (internal radius = ∼1.5 Å). The size of the K^+ cation also enables it to overcome the thickness of the macrocycle, which is estimated to be 3.2 Å based on the crystal structures of the K^+ complexes of receptors **10** and **11**.

The Issue of Electrostatics: (a) Pentafluorophenyl-Sidearmed Complexes, 12 M^+. Compounds **11** and **12** are identical except that the aromatic rings of the latter are perfluorinated. Although the van der Waals radii of aryl H (1.05 Å) and F (1.35 Å,[56] 1.47 Å[57]) differ slightly, **11** and **12** are essentially isosteres. Their π-donicities differ dramatically, however (see calculated electrostatic potential surfaces, Figure 2, panel e). For simplicity, the surfaces were calculated for toluene and for pentafluorotoluene rather than the entire side chain. The red color represents negative, cation-attracting density and is calculated for toluene to be near the arene's center. In contrast, pentafluorotoluene is substantially positive (blue = positive) at the center of the aromatic ring.

(b) Naphthyl-Sidearmed Receptor Complexes, 13·M^+. There are two, nearly equivalent aromatic subunits in each sidearm naphthyl group of **13**. Either may serve as a binding site for alkali metal cations in each side chain. Computational studies of the Na^+·naphthalene complex have been reported.[58,59] The calculated gas-phase binding energy for Na^+·naphthalene was 28.7 kcal/mol compared to a value for Na^+·benzene of 27.1 kcal/mol. In these calculations, the centroid of either of the six-membered rings, rather than the overall molecular center, was found to be the preferred binding site for Na^+. Thus, Na^+ could be aligned with either benzo ring in a π-complex of **13**. In fact, π-complexation is not observed in the K^+·**13** complex; instead, the sidearms are extended in a fashion similar to that of **12**·K^+ (Figure 7). The cation in both **12**·K^+ and **13**·K^+ is complexed by the anion rather than a π-donor. The observation of a non-π complex (K^+·**13**) in this case may be due to steric interactions because naphthalene is significantly larger than benzene.

Steric Effects. High-level quantum mechanical (gas phase) calculations performed on the indole-π·Na^+ complex predict that the metal cation will be aligned with the benzo, rather than the pyrrolo, centroid. In fact, the opposite is observed in the Na^+ and K^+ complexes of **7** (Figure 2d). What is the explanation for the discrepancy between *ab initio* calculations and our experimental results? One possibility is that the numerous theoretical calculations are in error because they ignore forces such as polarization effects[60] that are present in condensed phases.

(54) (a) Deakyne, C. A.; Meot-Ner, M. *J. Am. Chem. Soc*. **1985**, *107*, 474−479. (b) Mavri, J.; Koller, J.; Hadži, D. *J. Molecular Struct. (THEOCHEM)* **1993**, *283*, 305−312. (c) Kim, K. S.; Lee, J. Y.; Lee, S. J.; Ha, T.-K.; Kim, D. H. *J. Am. Chem. Soc*. **1994**, *116*, 7399−7400. (d) Caldwell, J. W.; Kollman, P. A. *J. Am. Chem. Soc*. **1995**, *117*, 4177−4178. (e) Basch, H.; Stevens, W. J. *J. Molecular Struct. (THEOCHEM)* **1995**, *338*, 303−315. (f) Lee, J. Y.; Lee, S. J.; Choi, H. S.; Cho, S. J.; Kim, K. S.; Ha, T.-K. *Chem. Phys. Lett*. **1995**, *232*, 67−71. (g) Chipot, C.; Maigret, B.; Pearlman, D. A.; Kollman, P. A. *J. Am. Chem. Soc*. **1996**, *118*, 2998−3005. (h) Pullman, A.; Berthier, G.; Savinelli, R. *J. Comput. Chem*. **1997**, *18*, 2012−2022. (i) Roelens, S.; Torriti, R. *J. Am. Chem. Soc*. **1998**, *120*, 12443−12452. (j) De Sant'Anna, C. M. R.; Bicca de Alencastro, R.; Barreiro, E. *J. THEOCHEM* **1998**, *429*, 217−227. (k) De Sant'Anna, C. M. R.; De Alencastro, R. B.; Barreiro, E. *J. THEOCHEM* **1999**, 167−180. (l) Tan, X. J.; Jiang, H. L.; Zhu, W. L.; Chen, K. X.; Ji, R. Y. *J. Chem. Soc., Perkin Trans. 2* **1999**, 107−112. (m) Zhu, W.-L.; Jiang, H.-L.; Puah, C. M.; Tan, X.-J.; Chen, K.-X.; Cao, Y.; Ji, R.-Y. *J. Chem. Soc., Perkin Trans. 2* **1999**, 2615−2622. (n) Minoux, H.; Chipot, C. *J. Am. Chem. Soc*. **1999**, *121*, 10366−10372. (o) Eriksson, M. A. L.; Morgantini, P.-Y.; Kollman, P. A. *J. Phys. Chem*. B **1999**, *103*, 4474−4480.

(55) (a) Burley, S. K.; Petsko, G. A. *FEBS* **1986**, *203*, 139−143. (b) Singh, J.; Thornton, J. M. *J. Mol. Biol*. **1990**, *211*, 595−615. (c) Scrutton, N. S.; Raine, A. R. C. *Biochem. J*. **1996**, *319*, 1−8.

(56) Emsley, J. *The Elements*, 2nd ed.; Clarendon Press: Oxford, 1991.

(57) Bondi, A. *J. Phys. Chem*. **1964**, *68*, 441−451.

(58) Mecozzi, S.; West, A. P., Jr.; Dougherty, D. A. *J. Am. Chem. Soc*. **1996**, *118*, 2307−2308.

(59) Dunbar, R. C. *J. Phys. Chem. A* **1998**, *102*, 8946−8952.

One may view the theoretical calculations as being limited by both the gas phase and the simplicity of the models. Alternately, one may consider the natural systems complicated by such interactions as H-bond formation and crystal packing forces. Indeed, issues such as solvation energies are not directly addressed by either gas-phase calculations or X-ray crystal structure determination. The orientation of Na^+ or K^+ proximate to the pyrrolo centroid is clear from the solid-state structures of **7**·M^+ complexes. We note that in all cases, the anion forms a hydrogen bond with the indole nitrogen, which is, of course, located on the pyrrolo subunit. Thus the cation−anion separation is minimized when the pyrrolo subunit serves as the π-donor. We estimate from CPK molecular models and the results of the *ab initio* calculations that the cation−anion separation would be increased ∼0.3 Å if the benzo centroid, rather than the pyrrolo subunit, coordinated Na^+ or K^+.

Presumably, the arene geometry in **7**·M^+ complexes is optimized not just for the cation−π interaction but also forces such as dipole−dipole, van der Waals, and steric interactions. Even in such simple receptor systems as **7**, **10**, and **11**, the overall conformation is controlled by countless intra- and intermolecular contacts. Among these, steric factors may be playing a critical role in determining the experimentally observed arene positions. The indole rings pack tightly against the crown ether (Figure 2, panels a and b) and are tilted, in the most extreme case (**7**·NaI) by over 26°. The observed indole·M^+ geometry in our lariat ether crystal structures could be determined by the limited steric accessibility of the ring bound cation.

Cation−π interactions are largely electrostatic effects. The binding energy between a cation and an arene is therefore dependent on the distance between the aromatic ring and the alkali metal cation. In complexes of **7**, the smaller pyrrolo unit can more closely approach the bound alkali metal when the cation is partially buried. Thus, the pyrrolo subunit of indole may be more accessible to a cation when it is bound within the crown ether.

Steric hindrance may also explain the *antiperiplanar* sidearm conformations (extended away from the macroring) that are observed for complexes of **7**·$NaPF_6$, **9**·NaI, **10**·NaI, **11**·NaI, and **13**·KI. When Na^+ is bound by the receptors, the crown more fully envelops the cation and hinders access of the arene. When K^+ is bound, the macroring enlarges (relative to bound Na^+) and only very large naphthalene fails to coordinate the cation. Thus, a combination of cavity size, cation size, macroring thickness, and arene size all play a role in dictating the observed complex conformations.

Conclusion

We present here the first solid-state structural evidence that demonstrates alkali metal cation−π interactions for a family of systematically varied, biologically relevant arenes. Cation−π sandwich coordination with K^+ is demonstrated for benzene, phenol, and indole and sodium−π complexation is documented for indole. In the latter case, solution NMR studies support the inferences drawn from the solid-state structures. In general, the observed cation−π interactions correlate well with theoretical predictions. The solid-state structures for indole-side-chained **7**·M^+ complexes contrast with the calculations, but the binding preference for the pyrrolo, over the benzo, subunit of indole may be understood to result from steric interactions. The latter is a very important observation because it demonstrates that the cation−π interaction is not only powerful but also versatile and may be observed even when cation−π geometry is not optimal. Such constraints may occur frequently in peptides and proteins containing tryptophan.

Experimental Section

^{1}H NMR spectra were recorded at either 300 or 500 MHz in $CDCl_3$ unless otherwise specified. Chemical shifts are reported in ppm (δ) downfield from internal TMS. NMR data are recorded as follows: chemical shift, peak multiplicity (b = broad; s = singlet; d = doublet; t = triplet; m = multiplet, bs = broad singlet, etc.), integration, and assignment. Infrared spectra were recorded in KBr unless otherwise noted and were calibrated against the 1601 cm^{-1} band of polystyrene. Melting points were determined on a Thomas-Hoover apparatus in open capillaries and are uncorrected. Thin layer chromatographic (TLC) analyses were performed on silica gel HLO F-254 (0.25 mm thickness), Scientific Adsorbents, Inc. Preparative chromatography columns were packed with silica gel from Merck (230−400 mesh, 60C). Chromatotron chromatography was performed on a Harrison Research Model 7924 Chromatotron with 1, 2, or 4 mm thick circular plates (Alltech).

All reactions were conducted under dry N_2 unless otherwise noted. All reagents were the best grade commercially available and were distilled, recrystallized, or used without further purification, as appropriate. Crystals suitable for X-ray analysis were prepared from commercially available solvents and salts were used without further purification. Combustion analyses were performed by Atlantic Microlab, Inc., Atlanta, GA, and are reported as percents.

Diaza-18-crown-6, **1**, was prepared according to a previously published procedure.[27]

***N,N′*-Di-*n*-propyl-4,13-diaza-18-crown-6**, **2,** was prepared as previously described.[8]

***N,N′*-Diallyl-4,13-diaza-18-crown-6**, **3**, was prepared as previously described.[8]

***N,N′*-Dipropargyl-4,13-diaza-18-crown-6**, **4**, was prepared as previously described.[8]

***N,N′*-Dibenzyl-4,13-diaza-18-crown-6**, **5**, was prepared as previously described.[28]

***N,N′*-Bis-(1-naphthylmethyl)-4,13-diaza-18-crown-6**, **6**, was prepared as previously described.[61]

***N,N′*-Bis(2-(3-indolyl)ethyl)-4,13-diaza-18-crown-6, 7.** Diaza-18-crown-6 (0.187 g, 0.712 mmol) and 3-(2-bromoethyl)indole (0.319 g, 1.42 mmol) were heated with Na_2CO_3 (0.377 g, 3.56 mmol) and NaI (0.011 g, 0.071 mmol) at reflux in CH_3CN (15 mL) for 24 h. The reaction mixture was filtered and concentrated *in vacuo*. The resulting residue was dissolved in CH_2Cl_2 and washed with H_2O (3 × 15 mL). The organic phase was dried with MgSO4 (anhydrous), filtered, and concentrated in vacuo to give a yellow solid. Compound **7** was isolated as a light yellow solid after recrystallization from ethanol (0.206 g, 53% yield), mp 129−131 °C. ^{1}H NMR (acetone-d_6, 0.03% TMS): 2.83−2.89 (m, $-CH_2CH_2-$ and $-N(CH_2)_2-$, 16H), 3.56 (s, $-OCH_2CH_2O-$, 8H), 3.61 (t, $-OCH_2CH_2N-$, 8H), 6.99 (t, indole-H5, 2H), 7.07 (t, indole-H6, 2H), 7.24 (s, indole-H2, 2H), 7.36 (d, indole-H7, 2H), 7.58 (d, indole-H4, 2H), 9.98 (s, indole-H1, 2H). Anal. Calcd for $C_{32}H_{44}N_4O_4$: C, 70.04; H, 8.08; N, 10.21. Found: C, 69.75; H, 8.05; N, 10.05.

Crystallization of 7 and 7·KI. Receptor **7** was dissolved in acetone at ambient temperature. Slow evaporation of the solvent over several weeks gave light yellow crystals of **7**. The complex was obtained by dissolving **7** and an equivalent amount of KI in Me_2CO. Yellow crystals of the complex formed within 24 h.

1-Methyl-3-(2-bromoethyl)indole was prepared as previously reported.[62]

***N,N′*-Bis(2-(3-*N*-methylindolyl)ethyl)-4,13-diaza-18-crown-6, 8.** Diaza-18-crown-6 (0.55 g, 2.1 mmol), 1-methyl-3-(bromoethyl)indole (1.0 g, 4.2 mmol), Na_2CO_3 (5.0 g, 45 mmol), and 10 mg of KI were heated at reflux in CH_3CN (50 mL) for 36 h. The mixture was cooled,

(60) (a) Caldwell, J. W.; Kollman, P. A. *J. Am. Chem. Soc*. **1995**, *117*, 4177−4178. (b) Cubero, E.; Luque, F. J.; Orozco, M. *Proc. Natl. Acad. Sci. U.S.A.* **1998**, *95*, 5976−5980.

(61) Meadows, E. S.; De Wall, S. L.; Barbour, L. J.; Fronczek, F. R.; Kim, M.-S.; Gokel, G. W. *J. Am. Chem. Soc.* **2000**, *122*, 3325−3335.

(62) Murillo, O.; Abel, E.; Maguire, G. E. M.; Gokel, G. W. *J. Chem. Soc., Chem. Commun.* **1996**, 2147−2148.

filtered, and concentrated under reduced pressure. The residue was taken up in CH_2Cl_2 (100 mL), washed with H_2O (3 × 100 mL), dried (Na_2SO_4), and reduced in vacuo to a light yellow oil. Column chromatography (0−5% Et_3N, Me_2CO on silica gel) afforded **8** (0.56 g, 46%) as a yellow oil. ^{1}H NMR (acetone-d_6): 2.85 (m, 16H, NCH_2CH_2Ind, NCH_2CH_2Ind, OCH_2CH_2N), 3.59 (m, 16H, OCH_2CH_2N, OCH_2CH_2O), 3.72 (s, 6H, CH_3−N), 7.03 (s, 2H, indole H2), 7.04 (t, J = 7.8, 2H, indole H5), 7.15 (t, J = 6.9, 2H, indole H6), 7.31 (d, J = 8.4, 2H, indole H4), 7.58 (d, J = 8.1, 2H, indole H7). ^{13}C NMR ($CDCl_3$): 136.3, 127.9, 126.4, 121.4, 118.8, 118.6, 112.8, 109.1, 70.6, 69.8, 56.6, 57.5, 53.9, 32.4, 22.9. HRMS (FAB) calcd for $C_{34}H_{49}N_4O_4$ $[M + H]^+$ 577.38, found 577.3775.

***N,N′*-Bis(2-(3-(5-methoxy)indolyl)ethyl)-4,13-diaza-18-crown-6, 9.** 5-Methoxytryptamine (0.20 g, 1.05 mmol), 1,2-bis(2-iodoethoxy)-ethane[63] (0.39 g, 1.05 mmol), Na_2CO_3 (1.0 g, 9.5 mmol), and 1 mg of KI were heated at reflux in CH_3CN (10 mL) for 40 h. The reaction was cooled and filtered, and the resulting solid was heated at reflux in EtOAc (50 mL) for 20 min. The mixture was filtered, and slow cooling (2 wk) of the filtrate afforded **9**·NaI as light yellow crystals (25 mg, 6%, mp 135−140 °C). ^{1}H NMR: 2.89 (m, 16H, NCH_2CH_2Ind, NCH_2-CH_2Ind, OCH_2CH_2N), 3.59 (m, 16H, OCH_2CH_2N, OCH_2CH_2O), 3.84 (s, 6H, CH_3−O−Ind), 6.81 (d, J = 9.0, 2H, indole H6), 7.02 (s, 2H, indole H4), 7.09 (s, 2H, indole H2), 7.20 (d, J = 9.0, 2H, indole H7), 8.34 (bs, 2H, indole NH). ^{13}C NMR ($CDCl_3$): 153.8, 131.4, 127.9, 123.2, 113.6, 111.9, 111.7, 100.5, 70.6, 70.4, 69.6, 56.2, 55.9, 55.5, 54.1, 22.7. HRMS (FAB) calcd for $C_{34}H_{49}N_4O_4$ $[M + H]^+$ 609.37, found 609.3676.

***N,N′*-Bis(2-(4-Hydroxyphenyl)ethyl)-4,13-diaza-18-crown-6, 10.** A mixture of 1,2-bis(2-iodoethoxy)ethane (6.74 g, 18.2 mmol), tyramine (2.5 g, 18.2 mmol), and Na_2CO_3 (105.99 g, 91.1 mmol) was heated at reflux in CH_3CN (50 mL) for 24 h. The mixture was cooled, filtered, and concentrated *in vacuo* to give an orange oil. The crude product was crystallized from acetone to give **10**·NaI as colorless crystals (0.390 g, 14%, mp 213−214 °C). ^{1}H NMR (CD_3OD, referenced to 3.31 ppm): 2.59−2.65 (m, phenol−CH_2−, 4H), 2.74−2.80 (m, −CH_2N-(CH_2)$_2$−, 12H), 3.63 (t, −NCH_2CH_2O−, 8H), 3.67 (s, −OCH_2CH_2O−, 8H), 6.69 (d, phenol, 4H), 6.96 (d, phenol, 4H). Anal. Calcd for $C_{28}H_{42}O_6N_2NaI$: C, 51.54; H, 6.49; N, 4.29. Found: C, 51.55; H, 6.51; N, 4.34. Free **10** was isolated by dissolving **10**·NaI (0.475 g) in CH_3CN (100 mL), washing with H_2O (3 × 25 mL), and then adding $CHCl_3$ (20 mL). The organic phase was dried with $MgSO_4$ and concentrated in vacuo. Recrystallization from absolute EtOH gave **2** as a light yellow solid (0.252 g, mp 176−178 °C). X-ray quality crystals of **10** were obtained by slow evaporation at room temperature of a saturated solution prepared in hot absolute EtOH solution.

Crystallization of 10·KI. Equivalent amounts of **10** and KI were dissolved in hot Me_2CO. Slow evaporation of the solvent over several days at room temperature yielded light yellow crystals of the complex.

***N,N′*-Bis(2-phenylethyl)-4,13-diaza-18-crown-6, 11.** A solution of (2-bromoethyl)benzene (0.727 g, 3.93 mmol), 4,13-diaza-18-crown-6 (0.515 g, 1.96 mmol), and Na_2CO_3 (0.519 g, 4.9 mmol) was stirred in refluxing CH_3CN (20 mL) for 24 h. The crude product was cooled to room temperature, filtered, concentrated in vacuo, redissolved in CH_2Cl_2 (100 mL), and washed with H_2O (3 × 15 mL); the organic phase was dried over $MgSO_4$, filtered, and concentrated again in vacuo to afford a yellow oil. The oil was purified by flash column chromatography (silica, 5% Et_3N in acetone (v/v)) to give the desired product as a colorless oil. After 24 h under high vacuum the oil solidified (0.554 g, 60% yield, mp 48−50 °C). ^{1}H NMR: 2.77 (s, crown−CH_2CH_2−phenyl, 8H), 2.86 (t, −NCH_2CH_2O−, 8H), 3.62 (m, −CH_2OCH_2−, 16H), 7.15−7.30 (m, phenyl, 10H). Anal. Calcd for $C_{28}H_{42}N_2O_4$: C, 71.46; H, 8.99; N, 5.95. Found: C, 71.20; H, 9.00; N, 5.90.

The complexes were obtained as follows. Equivalent amounts of **11** and NaI were mixed in EtOAc at ambient temperature. The solution was placed in a freezer at −20 °C. Slow evaporation of the solvent during several weeks afforded colorless crystals of **11**·NaI. Likewise, equivalent amounts of **11** and KI were mixed in EtOAc at ambient temperature. Slow evaporation of the solvent during several weeks afforded the complex as colorless crystals.

***N,N′*-Bis[2-(2,3,4,5,6-pentafluorophenyl)ethyl]-4,13-diaza-18-crown-6, 12. (a) 2,3,4,5,6-Pentafluorophenylacetyl Chloride.** To an ice-cold solution of 2,3,4,5,6-pentafluorophenylacetic acid (1.0 g, 4.42 mmol) in CH_2Cl_2 (50 mL) was added (dropwise) oxalyl chloride (2.0 M in CH_2Cl_2, 2.21 mL, 4.42 mmol) and anhydrous DMF (catalytic amount). The mixture was allowed to warm to ambient temperature during 1 h, and the CH_2Cl_2 was removed *in vacuo*. The resulting solid acid chloride was stored under N_2 until further use.

(b) *N,N′*-Bis[2-(2,3,4,5,6-pentafluorophenyl)ethylamide]-4,13-diaza-18-crown-6. To an ice-cold solution of 4,13-diaza-18-crown-6 (0.580 g, 2.21 mmol) and Et_3N (0.62 mL, 4.42 mmol) in CH_2Cl_2 (20 mL) was added (dropwise) an ice-cold solution of 2,3,4,5,6-pentafluorophenylacetyl chloride (1.08 g, 4.42 mmol) in CH_2Cl_2 (20 mL). After the addition, the mixture was stirred at room temperature (24 h), filtered, and concentrated *in vacuo* to an orange oil. Crystallization from EtOAc gave the desired amide (1.04 g, 70%) as a white solid, mp 132 °C.

***N,N′*-Bis[2-(2,3,4,5,6-pentafluorophenyl)ethyl]-4,13-diaza-18-crown-6, 12.** To a 0 °C THF solution (10 mL) of the bis(amide) obtained above (0.150 g, 0.221 mmol) was added BH_3·THF (1M, 10 mL), and stirring was continued for 24 h at ambient temperature. The mixture was concentrated in vacuo, HCl (6 M, 10 mL) was added, and the solution was heated at reflux for 30 min, cooled gradually to 0 °C, and made basic by addition of NaOH pellets. The basic solution was extracted with EtOAc, dried over anhydrous MgSO4, filtered, and concentrated in vacuo. Compound **12** was isolated (0.124 g, 86%) as a white solid, mp 61−62 °C. ^{1}H NMR: 2.73−2.86 (m, −CH_2-NCH_2CH_2−perfluorophenyl, 16H), 3.56 (t, −NCH_2CH_2O−, 8H), 3.58 (s, −OCH_2CH_2O−, 8H). Anal. Calcd for $C_{28}H_{32}F_{10}N_2O_4$: C, 51.69; H, 4.96; N, 4.31. Found: C, 51.50; H, 5.04; N, 4.19.

A nearly saturated ethyl acetate solution was prepared of **12**. Slow evaporation during several weeks gave crystals of **12** suitable for X-ray analysis. To obtain the complex,1 equiv of **12** (40 mg) was combined with KI (11 mg, 1 equiv) in EtOAc. Colorless crystals were obtained by slow evaporation over 7 days. Anal. Calcd for $C_{36}H_{46}N_2O_4KI$: C, 58.69; H, 6.29; N, 3.80. Found: C, 58.95; H, 6.34; N, 3.81.

2-(1-Naphthyl)ethyl *p*-toluenesulfonate was prepared from 2-(1-naphthyl)ethanol by a published procedure;[64] its physical properties were identical to those previously reported.[65]

***N,N′*-Bis-(2-(1-naphthyl)ethyl)-4,13-diaza-18-crown-3, 13.** Diaza-18-crown-6 (0.21 g, 0.8 mmol), 1-(2-*p*-tosylethyl)naphthalene (0.52 g, 1.6 mmol), and Na_2CO_3 (0.4 g, 6.4 mmol) were heated at reflux in MeCN (20 mL) for 72 h. The mixture was cooled, filtered, and concentrated *in vacuo*, and the residue was taken up in CH_2Cl_2 (100 mL), washed (3 × 100 mL H_2O), dried (Na_2SO_4), and concentrated *in vacuo* to afford a clear oil. Column chromatography (0−3% Et_3N in Me_2CO on silica gel) yielded **13** (0.28 g, 61%) as a colorless oil. ^{1}H NMR (acetone-d_6): 2.85 (m, 12H, OCH_2CH_2N, NCH_2CH_2naph), 3.23 (t, J = 6.9, 4H, naphCH_2CH_2N), 3.56 (m, 16H, OCH_2CH_2O, OCH_2CH_2O), 3.68 (m, 20H, OCH_2CH_2N, OCH_2CH_2O), 7.38 (m, 8H, naphth), 7.73 (t, 2H, J = 3.6, naphth), 7.87 (d, 2H, J = 7.8, naphth), 8.12 (d, J = 8.1, 2H, naphth). ^{13}C NMR (acetone-d_6) 138.3, 135.3, 133.3, 129.9, 127.9, 127.8, 127.0, 126.8, 126.6, 125.1, 71.7, 71.3, 58.0, 55.3, 32.2. **13** (40 mg) was combined with 11 mg (1 equiv) of KI and dissolved in EtOAc. Colorless crystals (mp 171−173 °C) were obtained by slow evaporation over 7 days. Anal. Calcd for $C_{36}H_{46}N_2O_4KI$: C, 58.69; H, 6.29; N, 3.80. Found: C, 58.95; H, 6.34; N, 3.81.

X-ray Crystallography. Data were collected at 173(1) K on a Bruker SMART CCD diffractometer (ω scan mode Mo K_I radiation, λ = 0.7107 Å). Data were corrected for absorption using the program SADABS.[66] Structure solution and refinement proceeded similarly for all structures (SHELX-97 software[67] using the X-Seed[68] interface). Direct methods yielded all non-hydrogen atoms of the asymmetric unit. These atoms were refined anisotropically (full-matrix least-squares

(63) Kulstad, S.; Malmsten, L. A. *Acta Chem. Scand*. **1979**, *B33*, 469−74.

(64) Saari, W. S.; Schwering, J. E.; Lyle, P. A.; Smith, S. J.; Engelhardt, E. L. *J. Med. Chem*. **1990**, *33*, 2590−5.

(65) (a) Bentley, M. D.; Dewar, M. J. S. *J. Am. Chem. Soc*. **1970**, *92*, 3996−4002. (b) Cram, D. J.; Dalton, C. K. *J. Am. Chem. Soc*. **1963**, *85*, 1268−1273.

(66) Blessing, R. H. *Acta Crystallogr*. **1995**, *A51*, 33−38.

method on F^2). Hydrogen atoms were placed in calculated positions with their isotropic thermal parameters riding on those of their parent atoms. When structures required modeling of disorder, the disordered hydrogen atoms were not placed. Mean planes of the macrocycles were calculated with PARST.[69] All X-ray structure figures were prepared with X-Seed and POV-Ray.[70]

Quantum Mechanical Calculations. The electrostatic potential surfaces were calculated by performing a full *ab initio* geometry optimization of the relevant aromatic molecule. The 6-31G** basis set was used as implemented by SPARTAN 5.0 or PC Spartan Pro 1.0.3 (Wavefunction, Inc.). An electron density surface was calculated for 0.002 electron/Å and the electrostatic potential was mapped onto the surface. All potential energy mapping was completed in the range of +25.0 kcal/mol to −25.0 kcal/mol. The blue color signifies a positive potential energy equal to or greater than +25.0 kcal/mol. A red color denotes an equivalent negative (−25 kcal/mol) potential energy. The binding energy of Na^+ complexes of the aromatic molecules was performed at the 6-31G** level of theory for both Na^+ and the aromatic group.

Titration Studies. A 0.5 M solution of NaI in acetone-d_6 (100%) was prepared in a 1 mL volumetric flask. The NaI was dried for 24 h in a vacuum oven at 100 °C. In a small, predried glass vial the diindole receptor, **7** (5 mg), was dissolved in 1 mL of acetone-d_6 (100%). The solution was transferred to a 5 mm NMR tube and then diluted to 2 mL with acetone-d_6. The final concentration of the solution of diindole receptor, **7**, was 5 mM.

Data were collected using Gemini 2300 (Varian, Inc.) at a frequency of 300 MHz. The NMR probe temperature was set to 25 °C. The sample tube was inserted into the spectrometer and allowed to equilibrate with the probe temperature. Each spectrum was obtained by collecting 16 transients. The signal from residual acetone in the solvent was used as the reference (2.05 ppm). Each spectrum was collected after adding a 1 μL aliquot of the 0.5 M NaI solution. Mixing of the titrant in the sample tube was accomplished by inverting the tube several times. A total of 25 data points were collected by this method. Identical results were obtained for the titration of a 10 mM sample of **7** with 1.0 M NaI solution in acetone-d_6. Assignment of the resonances in the spectra was possible for all protons. However, the resonances from the protons in the ethylene sidearm and those next to the nitrogens in the crown ether overlapped over the course of the titration making unequivocal assignment of these protons impossible.

2D-NMR Experiments. Experiments were done using either a Varian or Bruker 500 MHz NMR spectrometer. Both COSY and NOESY experiments were performed on a 10 mM solution of the indole receptor, **7**, in acetone-d_6. The total solution volume was 750 μL. The experiments were also carried out using the same concentration of **7** ([**7**] = 10 mM) and 1 equiv of NaI ([NaI] = 10 mM). Prior to doing the NOESY experiments the sample solutions were degassed by sonication. Experiments were carried out at 25 °C.

Crystal data for 7 (first crystal form): M = 548.71; light yellow rhombohedroid, 0.50 × 0. 50 × 0.45 mm^3; monoclinic, $P2_1/c$; a = 18.0798(9) Å, b = 12.1004(6) Å, c = 14.5384(7) Å, β = 110.2130(10)°; Z = 4; V = 2984.7(3) Å^3; D_c = 1.221 Mg/m^3; $2\theta_{max}$ = 54.32°, 17035 reflections collected, 6508 unique [R(int) = 0.0246]; final GoF = 1.033, $R1$ = 0.0458, $wR2$ = 0.1676, R indices based on 5039 reflections with $I > 2\sigma(I)$, μ = 0.081 mm^{-1}, minimum transmission factor = 0.763.

Polymorph of 7: M = 548.17; light brown parallelepiped, 0.30 × 0.25 × 0.20 mm^3; monoclinic, $P2_1/n$; a = 11.2857(8) Å, b = 31.408(2) Å, c = 12.7040(8) Å, β = 102.3590(10)°; Z = 6; V = 4398.7(5) Å^3; D_c = 1.243 Mg/m^3; $2\theta_{max}$ = 54.26°, 27176 reflections collected, 9655 unique [R(int) = 0.0554]; final GoF = 0.932, $R1$ = 0.0736, $wR2$ = 0.0625, R indices based on 4725 reflections with $I > 2\sigma(I)$, μ = 0.082 mm^{-1}, minimum transmission factor = 0.9757.

Crystal data for 7·NaI: M = 698.60; colorless rhombohedroids, 0.45 × 0.40 × 0.40 mm^3; monoclinic, $P2_1/n$; a = 17.3841(9) Å, b = 12.1395(6) Å, c = 15.4777(8) Å; β = 91.8540(10)°; Z = 4; V = 3264.6(3) Å^3; D_c = 1.421 Mg/m^3; $2\theta_{max}$ = 54.32°, 9866 reflections collected, 3609 unique [R(int) = 0.0176]; final GoF = 1.041, $R1$ = 0.0277, $wR2$ = 0.0649, R indices based on 3172 reflections with $I > 2\sigma(I)$, μ = 1.035 mm^{-1}, minimum transmission factor = 0.759.

Crystal data for 7·KI: M = 714.71; light yellow rhombohedroid, 0.40 × 0.30 × 0.20 mm^3; monoclinic, $C2/c$; a = 17.2370(10) Å, b = 12.0426(7) Å, c = 15.9510(9) Å, β = 90.2610(10)°; Z = 4; V = 3311.0(3) Å^3; D_c = 1.434 g/cm^3; $2\theta_{max}$ = 54.28°, 9687 reflections collected, 3620 unique [R(int) = 0.0323]; final GoF = 1.034, $R1$ = 0.0291, $wR2$ = 0.0682, R indices based on 3060 reflections with $I > 2\sigma(I)$, μ = 1.134 mm^{-1}, minimum transmission factor = 0.747.

Crystal data for 7·KPF6: M = 732.78; pale pink rhombohedroids, 0.40 × 0.35 × 0.30 mm^3; monoclinic, $P2_1/n$; a = 10.9698(8) Å, b = 13.0812(9) Å, c = 11.9828(9) Å; β = 95.0620(10)°; Z = 2; V = 1712.8(2) Å^3; D_c = 1.421 Mg/m^3; $2\theta_{max}$ = 54.18°, 10365 reflections collected, 3754 unique [R(int) = 0.0210]; final GoF = 1.049, $R1$ = 0.0325, $wR2$ = 0.0842, R indices based on 1698 reflections with $I > 2\sigma(I)$, μ = 0.277 mm^{-1}, minimum transmission factor = 0.8972.

Crystal data for 7·$(HPF_6)_2$: M = 838.65; pale orange rhombohedroids, 0.40 × 0.30 × 0.25 mm^3; monoclinic, $P2_1/c$; a = 10.0769(16) Å, b = 17.045(3) Å, c = 11.2044(18) Å; β = 105.547(3)° ; Z = 2; V = 1854.0(5) Å^3; D_c = 1.502 Mg/m^3; $2\theta_{max}$ = 52.84°, 15372 reflections collected, 3787 unique [R(int) = 0.0433]; final GoF = 1.055, $R1$ = 0.0652, $wR2$ = 0.1844, R indices based on 1698 reflections with $I > 2\sigma(I)$, μ = 0.220 mm^{-1}, minimum transmission factor = 0.9171.

Crystal data for 10: M = 502.64; colorless rhombohedroid, 0.35 × 0.20 × 0.10 mm^3; monoclinic, $P2_1/c$; a = 8.1816(10) Å, b = 17.039(2) Å, c = 9.7101(12) Å, β = 101.142(2)°; Z = 2; V = 1328.1(3) Å^3; D_c =1.257 g/cm^3; $2\theta_{max}$ = 54.24°, 8248 reflections collected, 2926 unique [R(int) = 0.0679]; final GoF = 1.000, $R1$ = 0.0561, $wR2$ = 0.1062, R indices based on 1438 reflections with $I > 2\sigma(I)$, μ = 0.088 mm^{-1}, minimum transmission factor = 0.9700.

Crystal data for 10·NaI: M = 652.53; colorless rhombohedroid, 0.35 × 0.35 × 0.25 mm^3; tetragonal, $P43$; a = 10.0920(4) Å, c = 60.278(3) Å; Z = 8; V = 6139.2(5) Å^3; D_c = 1.412 g/cm^3; $2\theta_{max}$ = 54.38°, 37186 reflections collected, 13363 unique [R(int) = 0.0509]; final GoF = 1.161, $R1$ = 0.0499, $wR2$ = 0.0954, R indices based on 11815 reflections with $I > 2\sigma(I)$, μ = 1.098 mm^{-1}, minimum transmission factor = 0.6998.

Crystal data for 10·KI: M = 668.64; colorless rhombohedroid, 0.35 × 0.30 × 0.20 mm^3; monoclinic, $C2/c$; a = 19.8231(15) Å, b = 9.5298(7) Å, c = 17.4222(13) Å, β = 113.1490(10)°; Z = 4; V = 3026.2(4) Å^3; D_c = 1.468 g/cm^3; $2\theta_{max}$ = 54.38°, 9095 reflections collected, 3342 unique [R(int) = 0.0313]; final GoF = 0.904, $R1$ = 0.0335, $wR2$ = 0.0755, R indices based on 2468 reflections with $I > 2\sigma(I)$, μ = 1.237 mm^{-1}, minimum transmission factor = 0.6713.

Crystal data for 11·NaI: M = 668.53; colorless rhombohedroid, 0.30 × 0.30 × 0.25 mm^3; triclinic, $P\bar{1}$; a = 10.0425(19) Å, b = 10.0425(19) Å, c = 31.775(6) Å, α = 90.191(3)°, β = 98.094(4)°, γ = 90.485(3)°; Z = 4; V = 3236.7(10) Å^3; D_c = 1.372 g/cm^3; $2\theta_{max}$ = 54.54°, 20010 reflections collected, 13857 unique [R(int) = 0.0581]; final GoF = 1.144, $R1$ = 0.1055, $wR2$ = 0.2470, R indices based on 11404 reflections with $I > 2\sigma(I)$, μ = 1.046 mm^{-1}, minimum transmission factor = 0.7444.

Crystal data for 11·KI: M = 636.64; colorless rhombohedroids, 0.40 × 0.30 × 0.15 mm^3; monoclinic, $C2/c$; a = 19.9098(9) Å, b = 9.6181(4) Å, c = 17.2441(8) Å, β = 116.4390(10)°; Z = 4; V = 2956.8(2) Å^3; D_c = 1.430 g/cm^3; $2\theta_{max}$ = 54.24°, 8740 reflections collected, 3248 unique [R(int) = 0.0185]; final GoF = 1.046, $R1$ = 0.0231, $wR2$ = 0.0594, R indices based on 2982 reflections with $I > 2\sigma(I)$, μ = 1.258 mm^{-1}, minimum transmission factor = 0.6331.

Crystal data for 12: M = 650.56; colorless rhombohedroids, 0.25 × 0.25 × 0.10 mm^3; monoclinic, $P2_1/c$; a = 15.0714(17) Å, b = 9.5904(11) Å, c = 9.9806(11) Å, β = 95.185(2)°; Z = 2; V = 1436.7(3) Å^3; D_c = 1.504 g/cm^3; 2 θ_{max} = 54.22°, 8742 reflections collected, 3162 unique [R(int) = 0.0392]; final GoF = 0.887, $R1$ = 0.0406, $wR2$ = 0.0871, R indices based on 1821 reflections with $I > 2\sigma(I)$, μ = 0.143 mm^{-1}, minimum transmission factor = 0.9652.

Crystal data for 12·KI: M = 816.56; colorless rhombohedroids, 0.25 × 0.25 × 0.20 mm^3; triclinic, $P1$; a = 8.0839(6) Å, b = 8.2103(6)

(67) Sheldrick, G. M., 1997, University of Göttingen.
(68) Barbour, L. J., 1999, University of Missouri−Columbia. (http://www.lbarbour.com/xseed/).
(69) (a) Nardelli, M. *J. Appl. Crystallogr*. **1995**, *28*, 659. (b) Nardelli, M. *Comput. Chem*. **1983**, *7*, 95−8.
(70) http://www.povray.org.

Å, $c = 13.9553(11)$ Å, $\alpha = 97.9020(10)°$, $\beta = 115.0700(10)°$; $Z = 1$; $V = 813.38(11)$ Å^3; $D_c = 1.667$ g/cm^3; $2\theta_{max} = 54.22°$, 5052 reflections collected, 3482 unique [R(int) = 0.0207]; final GoF = 1.041, $R1$ = 0.0526, $wR2$ = 0.1311, R indices based on 3042 reflections with $I > 2\sigma(I)$, $\mu = 1.206$ mm^{-1}, minimum transmission factor = 0.7526.

Crystal data for 13 KI: $M = 736.75$; colorless rhombohedroids, $0.30 \times 0.20 \times 0.15$ mm^3; orthorhombic, *Cmca*; $a = 14.852(2)$ Å, $b = 7.6873(11)$ Å, $c = 30.609(4)$ Å; $Z = 6$; $V = 3494.7(9)$ Å^3; $D_c = 2.100$ Mg/m^3; $2\theta_{max} = 54.22°$, 10428 reflections collected, 2003 unique [R(int) = 0.0316]; final GoF = 1.176, $R1 = 0.0762$, $wR2 = 0.1866$, R indices based on 1698 reflections with $I > 2\sigma(I)$, $\mu = 1.612$ mm^{-1}, minimum transmission factor = 0.6433.

Acknowledgment. We thank the NIH (GM-36262) and the NSF (CHE-9805840) for grants that supported this work. We are also grateful for an ACS Division of Organic Chemistry fellowship, funded by Procter and Gamble, to E.S.M. The 2-dimensional NMR experiments were accomplished with the assistance of Drs. D. André d'Avignon and Janet Braddock-Wilking whom we thank.

JA003059E